Identification of Novel Natural Substrates of Fibroblast Activation Protein-alpha by Differential Degradomics and Proteomics

Authors

Hui Emma Zhang, Elizabeth J. Hamson, Maria Magdalena Koczorowska, Stefan Tholen, Sumaiya Chowdhury, Charles G. Bailey, Angelina J. Lay, Stephen M. Twigg, Quintin Lee, Ben Roediger, Martin L. Biniossek, Matthew B. O'Rourke, Geoffrey W. McCaughan, Fiona M. Keane, Oliver Schilling, and Mark D. Gorrell

Correspondence

m.gorrell@centenary.usyd.edu.au

Graphical Abstract

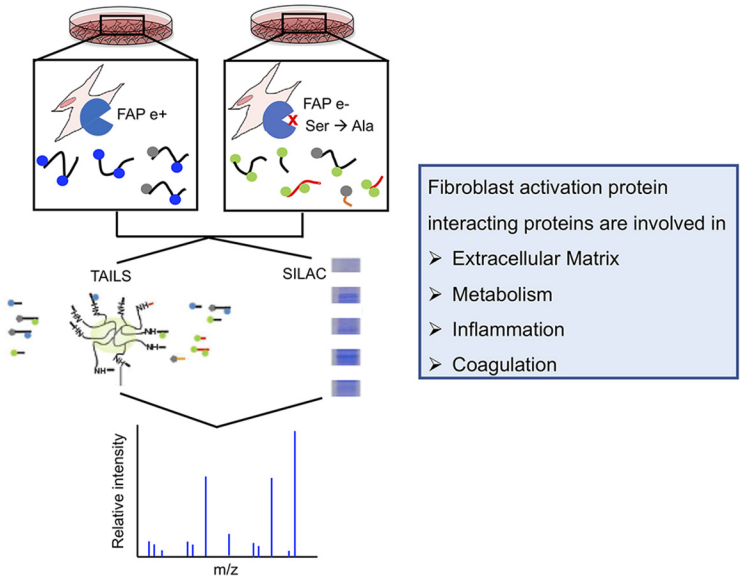

In Brief

Fibroblast activation protein-α (FAP) can hydrolyze the post-proline bond. We identified endogenous substrates of FAP in fibroblasts that were previously naive to both FAP and its proteolytic activity. FAP-dependent cleavage sites were identified in many extracellular matrix (ECM) and ECM-associated proteins including collagens and lysyl oxidase-like-1, and CSF-1, CXCL-5 and C1qT6. Quantitative proteomic analysis implicated FAP in ECM-cell interactions, coagulation and metabolism. This study greatly expands the repertoire of FAP substrates and shows that FAP has a role in coagulation in the mouse.

Highlights

- Natural substrates of FAP were identified using degradomic and proteomic techniques and FAP gene knockout mouse derived embryonic fibroblasts stably transduced with enzymatically active or inactive FAP.
- Terminal amine isotopic labelling of substrates (TAILS) based degradomics identified cleavage sites in collagens, and many other extracellular matrix (ECM) and associated proteins.
- Cleavages of lysyl oxidase-like-1, CXCL-5, CSF-1 and C1qT6 by FAP were confirmed *in vitro.*
- Differential metabolic labelling coupled with quantitative proteomic analysis implicated FAP in regulating proteins that are associated with ECM, ECM-cell interactions, coagulation, metabolism and wound healing.

Zhang et al., 2019, Molecular & Cellular Proteomics *18*, 65–85
January 2019
https://doi.org/10.1074/mcp.RA118.001046

Identification of Novel Natural Substrates of Fibroblast Activation Protein-alpha by Differential Degradomics and Proteomics*[S]

Hui Emma Zhang‡§‡‡‡, Elizabeth J. Hamson‡§‡‡‡, Maria Magdalena Koczorowska¶, Stefan Tholen¶, Sumaiya Chowdhury‡§, Charles G. Bailey‡§, Angelina J. Lay‡§, Stephen M. Twigg§‖, Quintin Lee‡§, Ben Roediger‡§, Martin L. Biniossek¶, Matthew B. O'Rourke‖**, Geoffrey W. McCaughan‡§, Fiona M. Keane‡§, Oliver Schilling‡‡§§¶¶§§§¶¶¶, and Mark D. Gorrell‡§‖§§§‖‖‖

Fibroblast activation protein-alpha (FAP) is a cell-surface transmembrane-anchored dimeric protease. This unique, constitutively active serine protease has both dipeptidyl aminopeptidase and endopeptidase activities and can hydrolyze the post-proline bond. FAP expression is very low in adult organs but is upregulated by activated fibroblasts in sites of tissue remodeling, including fibrosis, atherosclerosis, arthritis and tumors. To identify the endogenous substrates of FAP, we immortalized primary mouse embryonic fibroblasts (MEFs) from FAP gene knockout embryos and then stably transduced them to express either enzymatically active or inactive FAP. The MEF secretomes were then analyzed using degradomic and proteomic techniques. Terminal amine isotopic labeling of substrates (TAILS)-based degradomics identified cleavage sites in collagens, many other extracellular matrix (ECM) and associated proteins, and lysyl oxidase-like-1, CXCL-5, CSF-1, and C1qT6, that were confirmed *in vitro*. In addition, differential metabolic labeling coupled with quantitative proteomic analysis also implicated FAP in ECM-cell interactions, as well as with coagulation, metabolism and wound healing associated proteins. Plasma from FAP-deficient mice exhibited slower than wild-type clotting times. This study provides a significant expansion of the substrate repertoire of FAP and provides insight into the physiological and potential pathological roles of this enigmatic protease. ***Molecular & Cellular Proteomics 18: 65–85, 2019. DOI: 10.1074/mcp.RA118.001046.***

Fibroblast activation protein-alpha (FAP)[1] is a unique post-proline peptidase, which possesses both endopeptidase activity and dipeptidyl aminopeptidase (DPP) activity, allowing it to cleave a peptide bond two or more residues from the N terminus of a peptide or protein (1, 2). FAP is expressed at the cell surface and also shed. Both forms are enzymatically active and have similar substrate preferences (3). Although FAP has attracted much interest because of potential roles in fibrosis, cell migration and apoptosis and as a potential marker for many cancers (4–6), few of its natural substrates have been identified (1, 4, 7–11).

Only three of the identified endopeptidase substrates of FAP are physiological substrates, namely denatured type I collagen (1, 12), α2-antiplasmin (3) and fibroblast growth factor-21 (FGF-21) (8–10). By screening known DPP4 substrates (7), and then measuring cleavage in plasma (13), we have previously identified four physiological DPP-type substrates of FAP, namely neuropeptide Y (NPY), substance P, peptide YY (PYY) and B-type natriuretic peptide (BNP). NPY was found to be the most efficiently cleaved substrate of both human and mouse FAP, whereas all four peptides were found to be efficiently cleaved by endogenous DPP4, indicating that the *in vivo* degradomes of FAP and DPP4 differ (13).

Identification of additional FAP substrates is essential to fully elucidate its role as a protease. FAP is implicated in fibrinolysis because human α2-antiplasmin has 4-fold increased activity following FAP mediated cleavage (14). Inhibition of FAP increases the levels of active FGF-21 in obese mice more than in lean mice, demonstrating a metabolic benefit of FAP inhibition (15), which might be exploited for treating diabetes. Up-regulated expression of FAP is predominantly associated with disease states, including but not lim-

From the ‡Centenary Institute, the University of Sydney, Locked Bag No.6, Newtown, New South Wales, 2042, Australia; §Sydney Medical School, the University of Sydney Faculty of Medicine and Health, New South Wales, 2006, Australia; ¶Institute for Molecular Medicine and Cell Research, University of Freiburg, Freiburg, Germany; ‖Charles Perkins Centre, the University of Sydney, New South Wales, 2006, Australia; **Proteomics Core Facility, University of Technology Sydney, New South Wales, 2007, Australia; ‡‡Institute of Surgical Pathology, University Medical Center – University of Freiburg, Freiburg, Germany; §§BIOSS Centre for Biological Signaling Studies, University of Freiburg, Freiburg, Germany; ¶¶German Cancer Consortium (DKTK) and German Cancer Research Center (DKFZ), Heidelberg, Germany

Received August 28, 2018
Published, MCP Papers in Press, September 26, 2018, DOI 10.1074/mcp.RA118.001046

ited to tumorigenesis, fibrotic conditions and atherosclerosis (5, 6, 16, 17). Therefore, FAP is emerging as a promising marker of disease and much attention focuses upon exploiting this protease as a therapeutic target (4–6, 18). Nevertheless, the functions of FAP in both physiological and pathological processes remain unclear. Improved knowledge of the basic biology of FAP is necessary to broaden our perspective on potential outcomes of targeting this protease and predict potential impacts on the proteome when FAP enzyme activity is inhibited or ablated.

Several degradomic techniques have been developed for the discovery of physiological substrates of proteases for the DPP4 family (4, 19–22). The overall aim of this study was to identify novel substrates of FAP using an unbiased, global, degradomic technique (terminal amine isotopic labeling of substrates, or TAILS), a more targeted data mining approach, and a proteome comparison (stable isotope labeling by amino acids in cell culture, or SILAC). Through our identification of FAP substrates and subsequent investigation of the biological consequence of cleavage of these proteins, knowledge and understanding of the physiological role of FAP was enhanced.

EXPERIMENTAL PROCEDURES

Experimental Design and Statistical Rationale—A total of five replicate analyses were conducted for the differential proteomic investigation of the FAP enzyme-active (e+) and FAP enzyme-inactive (e−) mouse embryonic fibroblasts (MEFs) (see below for details of cell generation). A total of three replicate analyses were conducted for the differential N-terminomic investigation of the FAP e+ and FAP e− MEFs (see below for details of cell generation). Statistical analysis using linear models for microarray data (limma) (23) allows for the use of linear models to assess differential expression in the context of multifactor designed experiments. In addition, limma enables analyses of complex experiments involving comparisons between many peptides simultaneously in a small sample size, including multiple testing correction. Following the calculation of moderated-t-tests, proteins or cleavage sites with a p value < 0.05 and a quantitative alteration $> 50\%$ (either increase or decrease), were considered as being significantly affected.

Generation of FAP Enzyme-active (e+) and FAP Enzyme-inactive (e−) MEFs—MEFs were isolated from FAP gene knockout (GKO) mouse embryos aged 13.5 days. In this FAP GKO mouse strain, FAP has been deleted in both alleles and exons 3 to 26 are absent (24, 25). Primary MEFs were immortalized by transduction with the pFU-SV40-LTpuro lentiviral vector encoding the SV40 large T antigen then selected in puromycin (26). These MEFs were then divided into three cultures and transduced with a lentiviral vector pCCLteteGFP to express green fluorescent protein (GFP) as an empty vector control, or linked to one of two human FAP (hFAP) constructs using a picornaviral 2A peptide (27). PCR was used to amplify enzyme active (hFAP e+) and inactive (hFAP e−; serine724alanine) constructs from GFP-FAP (28) using the primers hFAP-5′BmgBI 5′-GTGGAAGAAAACCCCGGGCCCATGAAGACTTGGGTAAAAATCG-3′ and hFAP-3′BstBI 5′-AAAAGATTCGAAGTTTAAACTTAGTCTGACAAAGAGAAACAC-3′. PCR fragments (2324bp) were generated using Phusion polymerase (Finnzymes; Thermo Scientific, Waltham, MA) phosphorylated with T4 polynucleotide kinase (NEB, Ipswich, MA) and digested with BstBI. The pCCLteteGFP2Aluc2 lentiviral vector was cut with *BmgBI*/*ClaI* to clone in hFAP e+ and hFAP e− genes. Transduced MEFs were selected by GFP-based cell sorting using a BD Biosciences FACS Aria flow cytometer and expanded as pools. An endopeptidase activity assay was performed on the cells and secretomes of FAP e+ and FAP e− MEFs using the fluorogenic substrate Z-Gly-Pro-AMC (1 mM; Bachem, Bubendorf, Switzerland), in the presence or absence of a non-selective DPP inhibitor (Val-boro-Pro at 50 μM (kind gift from WW Bachovchin, Boston, MA) and a PEP-selective inhibitor (S17092 at 1 μM; Sigma-Aldrich, St Louis, MO).

Collection of Cell Conditioned Medium—Cell conditioned medium (CCM) was generated from three biological replicates of FAP e+ and e− MEF cell lines. Cells were grown in 15 cm dishes to a confluency of ~70% in 20 ml culture medium. After 16 h incubation in serum-free supplemented DMEM (Thermo Scientific) without phenol red, CCM was harvested in the presence of the following protease inhibitors: 0.01 mM trans-epoxysuccinyl-l-leucylamido (4-guanidino) butane (E64; Sigma-Aldrich), 5 mM ethylene-diaminetetraacetic acid (EDTA; Sigma-Aldrich) and 1 mM phenylmethylsulfonylfluoride (PMSF; Sigma-Aldrich). CCM was centrifuged at 1500 rpm and filtered using a 0.2 μm filter (Amicon; EMD Millipore, Billerica, MA) to remove dead cells and debris. HEPES buffer (Sigma-Aldrich) (pH 7.5) was added to a final concentration of 100 mM and the CCM mildly denatured and reduced with 5 mM dithiothreitol (DTT) (Sigma-Aldrich) at room temperature for 1–2 h. Free sulfide groups were alkylated by incubation with 20 mM iodoacetamide (IAA) (Sigma-Aldrich) for 2 h at room temperature in the dark, then 5 mM DTT was added for 15 min at room temperature to quench any remaining IAA.

Terminal Amine Isotopic Labeling of Substrates (TAILS)—TAILS was performed as described previously (29–31). Briefly, CCM was concentrated then precipitated with trichloroacetic acid. The protein pellet was re-solubilized in ice-cold 2 M guanidine hydrochloride using ultrasonication. After adjusting the pH to 7.5 using HEPES, the samples were reduced and alkylated again as described above. Protein was then differentially labeled with 40 mM heavy [d(2)^{13}C] or light [d(0)^{12}C] formaldehyde (Cambridge Isotope Laboratories, Andover, MA) in the presence of 40 mM sodium borohydride (for 18 h at 37 °C). After quenching excess reagents with 50 mM Tris (for 2 h at 37 °C), samples were mixed at equal amounts, acetone precipitated and resolubilized with 100 mM ice-cold NaOH. The pH was adjusted to 8 with HEPES-free acid and samples were digested overnight with mass spectrometry grade trypsin (Worthington, Lakewood, NY) at 37 °C. Labeled peptides were enriched by a negative selection step using a dendritic polyglycerol aldehyde polymer, as described (32). Blocked N-terminal peptides (unbound) were physically separated from the polymer-captured peptides via a 10 kDa molecular weight cut-off filter (Amicon; EMD Millipore). Flow through and filtrate were

[1] The abbreviations used are: FAP, fibroblast activation protein; APTT, activated partial thromboplastin times; BNP, B-type natriuretic peptide; CAF, cancer associated fibroblast; C1qT6, complement C1q tumor necrosis factor-related protein 6; CCL-2/MCP-1, monocyte chemoattractant protein-1; CCM, cell conditioned medium; CCR, C-C motif chemokine receptor; CN-I, type 1 collagen; CSF, colony-stimulating factor; CXCL, C-X-C motif chemokine ligand; DPP, dipeptidyl peptidase; DTT, 1,4-dithiothreitol; ECM, extracellular matrix; FGF, fibroblast growth factor; GFP, green fluorescent protein; GKO, gene knockout; IAA, iodoacetamide; IL, interleukin; limma, linear models for microarray data; LOX-L, lysyl oxidase homolog; MALDI, matrix assisted laser desorption ionisation; MEF, mouse embryonic fibroblast; MMP, matrix metalloproteinase; NPY, neuropeptide Y; PEP, prolyl endopeptidase; PMSF, phenylmethylsulfonylfluoride; PT, prothrombin times; PYY, peptide YY; SILAC, stable isotope labeling with amino acids in cell culture; TGF, transforming growth factor; TAILS, terminal amine isotopic labeling of substrates; TIMP, inhibitor of matrix metalloproteinase.

combined and desalted using a reverse phase C18 column (Sep-Pak, Waters, Milford, MA).

Stable Isotope Labeling by Amino Acids (SILAC) In Cell Culture—The SILAC protocol was performed as described (33). Briefly, MEFs were grown in heavy or light labeled DMEM (minus L-Arg and L-Lys; Silantes, Munich, Germany) supplemented with 10% dialyzed FCS and glutamine containing either L-arginine (Arg0) and L-lysine (Lys0) "light" or $^{13}C6\ ^{15}N4$ L-arginine (Arg10) and $^{13}C6\ ^{15}N2$ L-lysine (Lys8) "heavy" for at least five cell population doublings. After 16 h of seeding cells in heavy or light medium, CCM was collected as described above. Differentially labeled CCM was mixed at a ratio of 1:1 and concentrated to ~200 μl using Amicon® Ultra 50 ml 5 kDa centrifugal filters (EMD Millipore), 4000 g, 4 °C. Samples were run on 12–16% SDS-PAGE (Criterion Tris-HCL gel, Bio-Rad and NuPage® buffers, Thermo Scientific) and proteins visualized using a Colloidal Blue staining kit (Thermo Scientific). After destaining, gels were cut into 1 mm cubes and further destained with three rounds of 0.1 M ammonium bicarbonate, 50% acetonitrile and 50 mM ammonium bicarbonate then 100% acetonitrile, sonicating on ice. Gel pieces were digested with sequencing grade trypsin (Worthington) at pH 7.5, overnight at 37 °C. After digestion, peptides were eluted from the gel with 100% ethanol, samples were then concentrated using a Speed-vac concentrator (model 5301, Eppendorf, Hamburg, Germany) and desalted using a reversed phase C18 column (GRACE-VYDAC, Deerfield, IL).

Liquid Chromatography-MS/MS and Data Analysis—TAILS samples were then prefractionated by high performance liquid chromatography (HPLC) using a strong cation exchange column (SCX; PolyLC, Columbia, MD). Peptides were eluted in a linear gradient with increasing concentration of 5 mM KH_2PO 1 M KCl 25% acetonitrile pH 2.7; 10–14 fractions were collected and desalted using self-packed C18 STAGE tips (Empore; 3 M, St Paul, MN) (34). Differential proteomics samples were pre-fractionated by SDS-PAGE as described previously (31). For nanoflow-LC-MS/MS analysis, samples for quantitative proteomic comparison were analyzed on a Qstar Elite (AB Sciex, Framingham, MA) and TAILS samples on an Orbitrap XL (Thermo Scientific GmbH, Bremen, Germany) mass spectrometer. Both instruments were coupled to an Ultimate3000 micro pump (Thermo Scientific) with a flow rate of 300 nL/min each. Buffer A was 0.5% (v/v) acetic acid, and buffer B was 0.5% (v/v) acetic acid in 80% (v/v) acetonitrile (water and acetonitrile were at least HPLC gradient grade quality). A gradient of increasing organic proportion was used for peptide separation. Column-tips with 75 μm inner diameter and a length of 11 cm were self-packed with Reprosil-Pur 120 ODS-3 (Dr. Maisch, Ammerbuch, Germany). The MS operated in data dependent mode, with the SMART being used for the QSTAR Elite. For the Orbitrap XL, each MS scan was followed by a maximum of five MS/MS scans; and for the Qstar Elite three MS/MS scans.

Raw QSTAR LC-MS/MS data in wiff format (quantitative proteomic comparison, SILAC) was converted to the mzXML (35) format, using mzWiff (version 4.3.1, http://sourceforge.net/projects/sashimi/files/mzWiff%20(Analyst%20converter), with centroiding of MS1 and MS2 data, precursor charge determination, and deisotoping of MS2 data. X!Tandem (version 2013.09.01) (36) was used for spectrum to sequence assignment. The proteome database consisted of (1) mouse UniProt sequences (without isoforms) downloaded from UniProt on April 15th, 2016, (2) the sequence of human FAP, and (3) the contaminant database of MaxQuant (total of 50935 entries). It was appended with an equal number of shuffled decoy entries derived from the original human protein sequences. The decoy sequences were generated with the software DB toolkit (37). X!Tandem parameters for analysis of QSTAR data included: asymmetric precursor mass error of −50–150 ppm, fragment ion mass tolerance of 0.2 Da, tryptic cleavage specificity with no missed cleavage sites, residue modifications: cysteine carboxyamidomethylation (+57.02 Da), variable modifications were isotope-labeled (+6.02 Da) arginine and lysine. X!Tandem results were further validated by PeptideProphet (38). Peptides were assembled to proteins using ProteinProphet (39) at a false discovery rate of less than 1%. XPRESS was used for relative peptide and protein quantification (40). Mass tolerance for quantification was 0.1 Da. Ratios of each dataset were calculated as FAP-active/FAP-inactive and $\log_2$-transformed. Five biological replicates were analyzed. Prior to limma statistical analysis (see Statistical Rationale above), samples were mean normalized. No outlier removal was performed. Isoform quantification was solved by the well-established XPRESS algorithm, which assigns weights to peptides accordingly.

Raw Orbitrap-XL LC-MS/MS data (TAILS, stable isotope labeling with dimethylation) was converted to the mzXML (35) format, using msconvert (41) with centroiding of MS1 and MS2 data and deisotoping of MS2 data. For spectrum to sequence assignment X!Tandem (version 2013.09.01) (36) was used, with the proteome database described above. X!Tandem parameters for analysis of Orbitrap-XL data included: precursor mass error of ± 10 ppm, fragment ion mass tolerance of ± 0.4 Da, semi-ArgC specificity with up to three missed cleavages, static residue modifications: cysteine carboxyamidomethylation (+57.02 Da); lysine and N-terminal dimethylation (light formaldehyde 28.03 Da; heavy formaldehyde 34.06 Da or 36.08 Da; no variable modifications. These X!Tandem results were further validated by PeptideProphet at a confidence level of > 95%. XPRESS was used for relative peptide quantification (36, 38, 40). Mass tolerance for quantification was 0.015 Da. Ratios of each data set were calculated as FAP-active/FAP-inactive and $\log_2$-transformed. Three biological replicates were performed. Prior to limma statistical analysis (see Statistical Rationale above), samples were mean normalized. No outlier removal was performed. An in-house PERL computer script (downloadable at http://www.mol-med.uni-freiburg.de/mom/schilling/TAILS_v21_xpress-only/at_download/file) then filtered for peptides that had a non-tryptic N terminus generated. Like the original PICS procedure (42), the script then determines bioinformatically, through database lookup, the corresponding prime- or non-prime sequence. The script also used Uniprot and Gene Ontology annotation to distinguish secreted proteins. Web-PICS was used to generate heat-map style representation of protease specificity (43).

Recombinant Peptides and Proteins and MALDI-TOF-MS—Full-length recombinant proteins were purchased (Peprotech, Rocky Hill, NJ or R&D Systems, Minneapolis, MN), including human CCL-2 (hCCL-2; #300–04), mouse CCL-2 (mCCL-2; #250–10), mouse CXCL-5 (mCXCL-5; #250–17), human FGF-21 (#100–42). Recombinant synthetic peptides were synthesized by Mimotopes (Clayton, Australia) for substrate validation. If the potential cleavage site was a DPP cleavage event the first 15–20 amino acids of the mature N terminus of the candidate substrate were synthesized, as we have done previously (20, 21). Recombinant human FAP (rhFAP; #3715-S.E.; R&D Systems), produced in baculovirus/Sf21 cultures, consisted of 735 amino acids (Accession# Q12884; Leu26 to Asp760 with N-terminal polyhistidine tag). This is a soluble form because it lacks the N-terminal transmembrane domain.

Recombinant peptides and proteins at the stated amount were incubated with rhFAP or buffer control in 25 mM Tris and 0.25 M NaCl (pH 8.0) for up to 24 h at 37 °C. At each time point, a 1 μl sample of enzyme/substrate solution was pipetted onto the surface of a ground steel target plate, allowed to dry and then overlaid with 0.5 μl of sinapinic acid matrix solution (10 mg/ml in a solution of 50:50 0.1% trifluroacetic acid and 100% acetonitrile and then sonicated until completely dissolved). Matrix-Assisted-Laser-Desorption-Ionisation (MALDI) Mass Spectrometry analysis was performed as previously described (7, 13). Once dry, the target plate was loaded into a Bruker UltafleXtreme MALDI TOF/TOF (Bremen, Germany) and analyzed with

the following settings: Linear mode, Mass Range 5–50 kDa, Detector Gain 40×, Sample Rate 0.63 GS/s, Smartbeam Parameter "medium," Frequency 2000 Hz and realtime smoothing set to "high," Laser shots 1000 (or 5× 1000 shots for dilute samples). Once mass spectra were acquired, post processing was performed In Flex analysis (Bruker Daltonics, Germany) with TopHat baseline subtraction followed by spectral smoothing using 1 cycle of the Savitzsky Golay algorithm at a width of 5 *m/z*. Peak detection was performed manually by labeling the monoisotopic peak.

Immunoblotting—Whole cell lysates and CCM were made and protein concentration was quantified using the Micro BCA Protein Assay Kit (#3235; Thermo Scientific). 4–12% Bis-Tris SDS-PAGE (NP0323PK2; Thermo Scientific) and immunoblotting was performed as previously described (44). Primary antibodies were a goat polyclonal to mouse CSF-1 (AF416; R&D Systems) at 0.2 μg/ml and a rabbit polyclonal to LOX-L1 at 0.3 μg/ml (NBP1–82827; Novus Biologicals, Littleton, CO). Mouse monoclonal antibodies to GAPDH (G8795; Sigma-Aldrich) at 0.1 μg/ml and beta-actin (ab49900; Abcam, Cambridge, MA) at 0.1 μg/ml were internal loading controls. Band intensity was quantified with Image J software (National Institutes of Health, Bethesda, MD).

Flow Cytometry—Flow cytometry methodology has been described previously (28, 45, 46). FAP e+ and e− MEFs were fixed in 2% (v/v) paraformaldehyde and stained with primary antibody against human FAP (F19) at 2.99 μg/ml (46) or the antibody against CSF-1 at 4 μg/ml after cell permeabilization using 0.05% (w/v) saponin. Normal mouse IgG (#12–371B, EMD Millipore) at 2.99 μg/ml and goat IgG (AB-108-C; R&D Systems) at 4 μg/ml were used as negative controls, respectively. The gating strategies are shown in supplemental Fig. S1. A fluorescence signal from nonpermeabilized cells is indicative of membrane expression.

Immunofluorescence Staining, Confocal Microscopy and Real Time qPCR—The FAP e+ and e− MEFs were stained with the F19 antibody and imaged using a Leica TCS SP5 confocal microscope as described previously (44). Real time qPCR on DPP4, DPP8, and DPP9 were performed as described previously (47) using Taqman gene expression assays (Applied Biosystems; Thermo Scientific), with β-actin as a standard.

Leukocyte Migration Assays—Neutrophils and monocytes were isolated from mouse bone marrow as described previously (48, 49). Bones harvested from C57BL/6J mice were crushed in sort buffer (2.5% Fetal Bovine Serum [FBS, Hyclone, GE Life Sciences, Pittsburg, PA], 2 mM EDTA in PBS) followed by centrifugation at 500 × *g*, 5 min, 4 °C. For monocyte isolation, cells were then resuspended in 4 ml PBS and underlaid with 3 ml Histopaque® 1083 (Sigma-Aldrich) before centrifuging at 400 × *g*, 30 min, 22 °C without braking. The interface enriched with mononuclear leukocytes was carefully aspirated and washed twice in 10 ml sort buffer at 500 × *g*, 5 min, 4 °C. For neutrophil isolation, cells were immediately subjected to red blood cell lysis by adding 1.5 ml ACK lysis buffer (145 mM NH_4Cl, 0.1 mM EDTA, 12 mM $NaHCO_3$ in triple-distilled water) for 2.5 min at room temperature before washing twice in 10 ml sort buffer at 400 × *g*, 5 min, 4 °C. Cells were then stained at 4 °C for 50 min with the following antibodies: B220 PE and APC (clone RA3–6B2, BD Biosciences, San Diego, CA), CD115 PE (clone AFS98, eBioscience, San Diego, CA), Ly6C FITC (clone HK1.4, BioLegend, San Diego, CA) and/or Ly6G FITC and A647 (clone 1A8, BD). Cells were washed twice in 10 ml sort buffer at 400 × *g*, 5 min, 4 °C before resuspending in sort buffer containing 0.5 μg/ml DAPI (4′,6-Diamidino-2-Phenylindole dihydrochloride, #D1306 Invitrogen, Eugene, OR). Monocytes or neutrophils were subsequently sorted on a 7-laser Influx (BD) or 3-laser FACSAria II (BD), whereby DAPI- live cells were initially selected, followed by the exclusion of B220+ and Ly6G+ cells. Subsequently, for monocyte isolation, CD115+ monocytes were selected, and for neutrophil isolation, Ly6G+ neutrophils were selected. Cells were collected in 2 ml FBS before usage for transwell migration assay. CytoSelect™ 24-well cell migration assay with 5 μm pore size (CBA-102, Cell Biolabs, Inc., San Diego, CA) was performed according to the manufacturer's instructions (50). Sorted cells (1.5×10^6 cells/well) were added to the insert and chemoattractant was added to the lower well of the migration plate. To examine monocyte migration, mCCL-2 was pre-incubated with buffer or rhFAP at 37 °C for 24 h. Where FAP enzyme activity was inhibited, FAP inhibitor ARI-3099 (51) at 20 μM was preincubated with rhFAP for 20 min at 37 °C. To examine neutrophil migration, mCXCL-5 was preincubated at 37 °C for 24 h with buffer or rhFAP in the presence of plasma from FAP enzyme-negative gene knock-in (gki) mice (52). FAPgki mouse plasma contains naturally occurring proteases and cytokines and so is a physiological environment for analyzing substrate cleavage. Cells were allowed to migrate for 1.5 h at 37 °C, then cells from cells in the lower well, including cells on the underside of the membrane, were lysed and stained with the CyQuant® GR dye. Fluorescence was read with a fluorescence plate reader at 480 nm excitation/520 nm detection (POLARstar Omega, BMG Labtech). Chemotaxis index (fold change over the media control) was calculated.

Coagulation Assay—Wildtype (WT) and FAP GKO mice were anesthetized using isoflurane then blood was collected via cardiac puncture into tubes at a ratio of 9:1 blood:citrate (3.5%; v/v). Plasma were assayed for prothrombin time (PT) and activated partial thromboplastin time (APTT) by the Institute of Hematology, Royal Prince Alfred Hospital, Australia. Full blood counts on WT, DPP4 GKO and FAP GKO mice were performed by veterinary pathology diagnostic services of the University of Sydney.

Annotated spectra of the TAILS data and of the global quantitative proteome comparison are provided at MS-viewer (54). The experiments and the corresponding Search Keys are listed in supplemental Table S1.

RESULTS

Generation of FAP Enzyme-active (e+) and FAP Enzyme-inactive (e−) MEFs—To investigate the enzymatic activity of FAP with a focus on identifying novel natural substrates of FAP, cell lines suitable for proteomic and degradomic studies were designed and produced. Uniquely, we used FAP GKO cell lines so that substrates had no exposure to endogenous FAP. We have detected no compensatory changes in DPP8, DPP9 or DPP4 mRNA expression in FAP GKO mice (47). Three biological replicates of the FAP e+ and e− FAP MEF cell lines were generated. Confocal microscopy (Fig. 1*A*) and flow cytometry (Fig. 1*B*) indicated cell surface expression of human FAP and intracellular expression of GFP by the FAP e+ and FAP e− mouse cell lines. FAP e+ and FAP e− cells expressed similar amounts of hFAP mRNA, and no hFAP mRNA was detected in the empty vector control cells (Fig. 1*C*). Only whole live FAP e+ MEFs (Fig. 1*D*) and CCM (Fig. 1*E*) contained FAP enzyme activity. These data confirmed the MEF phenotypes and the serine to alanine catalytic inactivation of FAP.

Expression and activity levels of closely related proteases were then measured in these cell lines, because when one protease is downregulated, compensatory mechanisms might upregulate enzymes that have similar functions. Specifically, DPP4, DPP8, and DPP9 share DPP activity with FAP, and PEP

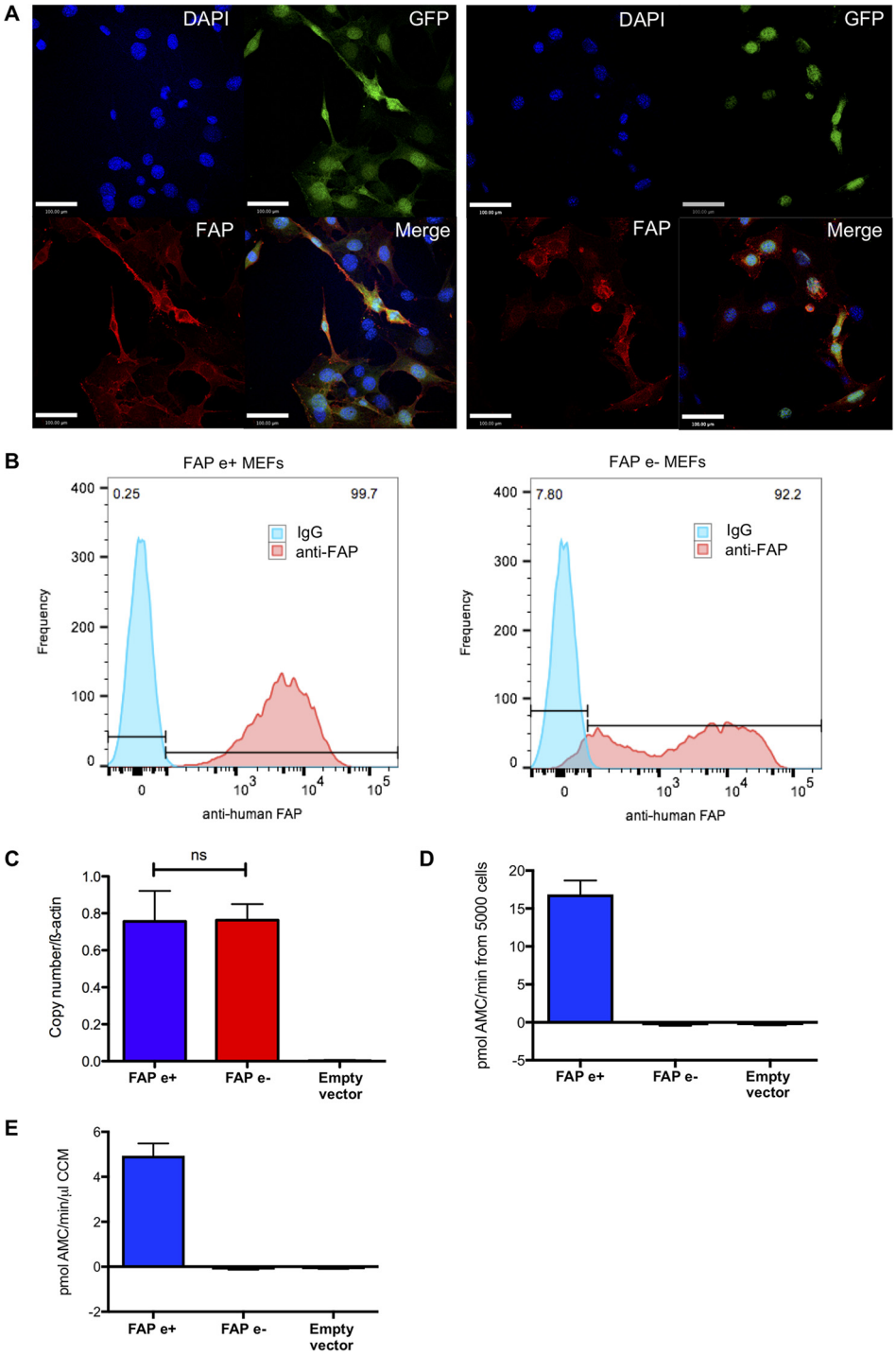

FIG. 1. **Validation of FAP expression in FAP e+ and FAP e− MEFs.** *A*, FAP e+ (left) and FAP e− (right) transduced MEFs stained with the F19 antibody that binds to human FAP (red). Cell nuclei were counterstained with DAPI (blue). Scale bars: 100 μm. Confocal microscopy images are representative of three replicate cell lines. *B*, F19 antibody stained cell surface FAP on FAP e+ (left; 99.7%) and FAP e− (right; 92.2%) MEFs by flow cytometry. Mouse IgG was used as a negative control. *C*, qPCR of FAP mRNA expression in FAP e+, FAP e− and empty vector control MEFs, normalized to the house keeping gene β-actin. Mean ± S.D.; $n = 3$. *D*, *E*, FAP enzyme activity of FAP e+, FAP e− and empty vector control MEFs was measured in a FAP-specific enzyme assay on whole live cells in PBS (*D*) and cell conditioned medium (CCM) harvested from MEFs after 16 h serum starvation (*E*). Mean ± S.E.; $n = 3$; ns = not significant.

exhibits comparable endopeptidase activity; although PEP, DPP8, and DPP9 are exclusively intracellular (2, 4, 44, 55, 56). We observed no significant difference in mRNA levels of *dpp8* or *dpp9*, and *dpp4* was downregulated to a small extent in the FAP e− MEFs compared with FAP e+ MEFs (supplemental Fig. S2*A*). PEP activity was not detected in the CCM (supplemental Fig. S2*B*), so it would be very unlikely that this protease influenced the degradomic analyses of MEF CCM.

TAILS N-terminome Analysis on Secretomes of FAP e+ and FAP e− MEF Cell Lines—To identify FAP-dependent proteolytic cleavage sites, we employed the TAILS method for an N-terminomic analysis of CCM produced by FAP e+ MEFs compared with FAP e− MEFs. Three biological replicate analyses were conducted. Identified N termini are summarized in supplemental Tables S2–S4.

In line with earlier TAILS studies (57), we focused on protein N termini that were identified in at least two replicates. Of those 1914 N termini, 1340 mapped to proteins that are annotated in Uniprot as being secreted but not exclusively in exosomes. Compared with previous N-terminomic studies on cultured cells, this was a high proportion of secreted or shed proteins (58). Therefore, our statistical analysis focused on cleavage sites in secreted or shed proteins.

To identify cleavage sites that significantly differ in their abundance depending on FAP activity, we employed limma statistics (59). Limma is superior to a classical Student's *t* test (*e.g.* with regard to multiple testing correction and prevention of false-positive discoveries) (60) in the analysis of omics-style data, which is characterized by a large number of analytes in a small number of biological replicates (Fig. 2). We chose the following criteria to distinguish significantly regulated cleavage sites: (1) limma moderated p value < 0.05 and (2) average increase or decrease in abundance by more than 50% (log2 (FAP-active/FAP-inactive) > 0.58 for increase; log2 (FAP-active/FAP-inactive) < -0.58 for decrease. These strict criteria highlighted 308 up-regulated and 278 downregulated cleavage sites upon increased FAP activity (limma statistics in supplemental Table S5). Log-transformed fold-change distributions before and after normalization appear in supplemental Fig. S3.

Proteases act in networks with strong interdependency (61). Often, altered activity of a protease under investigation has downstream and secondary effects, *e.g.* stemming from inactivation or activation of other proteases. The sequence specificity of a cleavage site is a useful criterion to distinguish direct substrates of a protease under investigation from downstream effects (62).

FAP predominantly acts as an amino-dipeptidase with a strong preference for P1 proline together with small amino acids (mostly glycine, to a lesser extent alanine) in P2 (63). Endoproteolytic activity has been reported as well (3), but in an *in vivo* or cell-contextual setting, endoproteolytic activity of FAP remains difficult to distinguish from primary cleavage

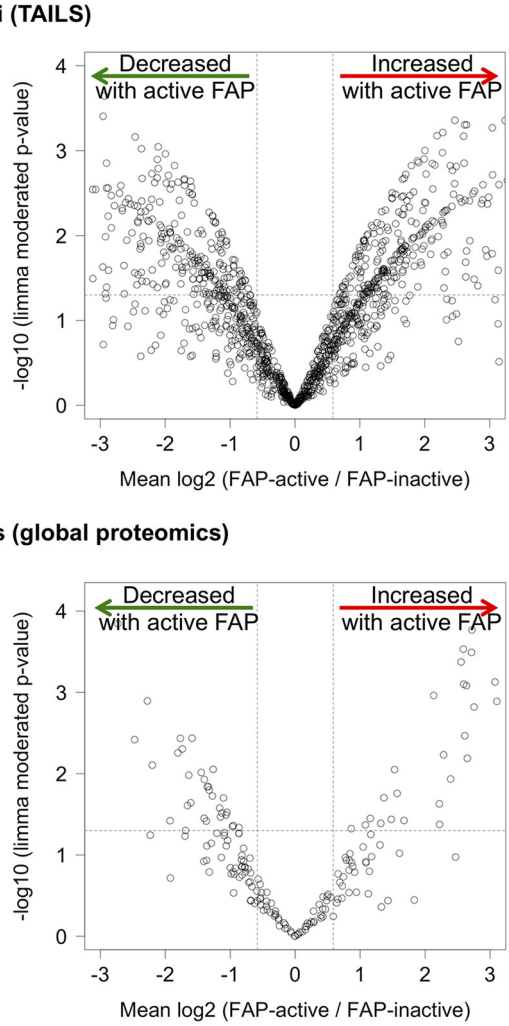

FIG. 2. **Proteomics and degradomics data.** Volcano plot representation of the comparisons of FAP-active and FAP-inactive MEF secretomes following limma analyses of TAILS (*A*) and SILAC (*B*; global proteomics).

by a different endoprotease (*e.g.* a matrix metalloprotease (MMP)), followed by processing of the neo N termini by FAP.

Specificity profiling of the 308 "upregulated" cleavage sites that depend upon FAP activity highlights a noticeable preference for P1 proline and P2 glycine (43) (Fig. 3*A* and 3*B*). These data correspond to the reported Gly-Pro cleavage site specificity of FAP (12, 63, 64). These data also provide some insight into the non-prime amino acids surrounding the cleavage site, including the unique observation of a preference for serine or threonine in P1′.

Identification of Candidate FAP Substrates by Parsing TAILS Data—In the set of 308 "upregulated" cleavage sites that depend on FAP activity, we focused on cleavage sites with a P1 proline to identify *bona fide* FAP substrates.

Candidate Substrates Exhibiting Postproline Cleavage—Following the criteria outlined above, 37 *bona fide* FAP cleavage sites were identified (Table I, supplemental Table S6).

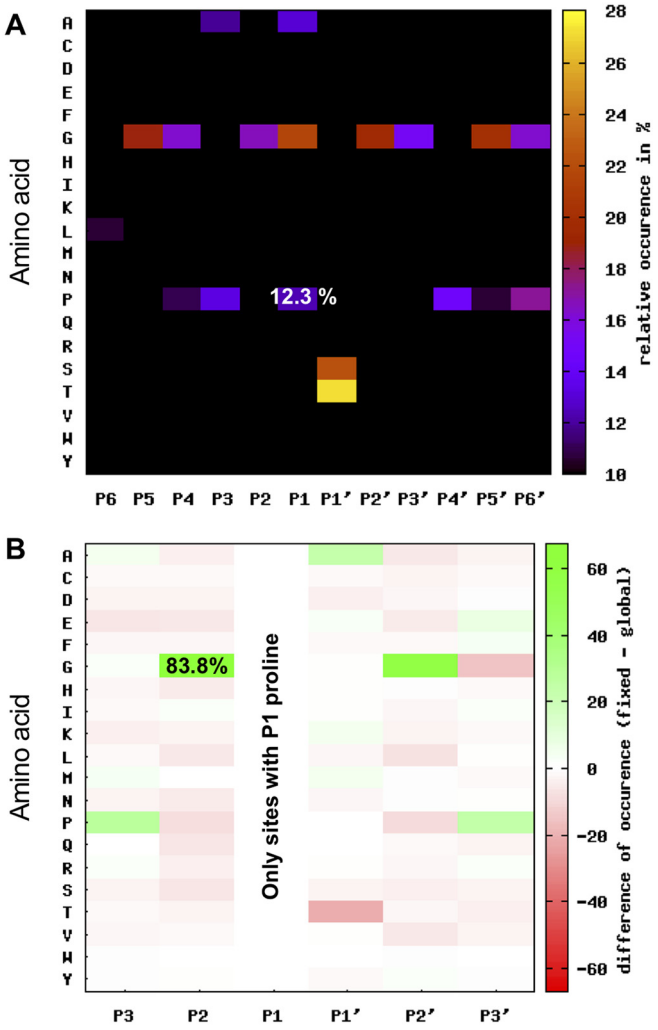

FIG. 3. **Understanding the cleavage site specificity of FAP.** Graphical representation of the FAP e+ secretome specificity profile of peptides following limma analysis of TAILS. *A*, A heatmap of the occurrence of amino acids in each position, P6-P6′, relative to the natural abundance levels of amino acids in the mouse (93). The cleavage site specificity of FAP shows preferences for proline (P) in P1 (12.3%). *B*, Dependence plot displaying the amino acid occurrence (%) at positions P3-P3′ when proline is fixed at position P1. There was an 83.8% likelihood of glycine in position P2 when proline is at P1.

Among the candidate substrates is type 1 collagen (CN-I), which is a well-known substrate of FAP (1, 12). Thus, identification of neo-N termini produced from cleavage events after a proline in CN-I from the FAP e+ secretome acted as an internal positive control and demonstrated the reliability of the TAILS method. Cleavage events were also observed in collagen types III and V.

Further FAP cleavage sites in extracellular matrix components were found in fibrillin-2 and extracellular matrix protein 1 (ECM-1). In fibrillin-2, the cleavage occurred at position 60, in the propeptide domain, after a Gly-Pro sequence. In ECM-1, cleavage occurred at position 142 after a Lys-Pro sequence, which renders a preceding cleavage by a different endoprotease likely. Cleavage of lysyl oxidase homolog 2 (LOX-L2) by FAP was seen near the genome-encoded N terminus at position 36 after a Tyr-Pro sequence that follows the signal peptide.

In addition, there was prominent processing of complement C1q tumor necrosis factor-related protein 6 (C1qT6) by FAP at position 26 after a Val-Pro sequence. After removal of the signal peptide, secreted C1qT6 commences with this Val-Pro sequence. Thus, FAP acts as an aminodipeptidase on C1qT6.

Lastly, TAILS provided evidence for processing by FAP of CXCL-5 at position 42, which is after an Ala-Pro sequence. CXCL-5 has an unusually long signal peptide of 40 residues, so Ala-Pro is the N terminus of secreted CXCL-5. Thus, FAP acts as an aminodipeptidase on CXCL-5.

Cleavage Sites Lacking a P1 Proline That Are Affected By FAP Activity—FAP activity had a strong effect on numerous cleavage sites that do not represent its known active site specificity. There are clear data that FAP can cleave post-alanine as well as post-proline (21, 22), but cleavage after other residues may be downstream effects of FAP rather than substrates directly hydrolyzed by FAP. Nevertheless, this "downstream degradome" constitutes an important aspect of FAP biology. For example, FAP activity leads to substantially elevated levels of MMP-1 in cancer-associated fibroblasts while simultaneously reducing the levels of tissue plasminogen activator (tPA) (63). MMP-1 and FAP co-operatively digest collagen (12).

Many neo-N termini lacking a P1 proline were affected by FAP activity (supplemental Table S5). These include the ECM proteins fibronectin, CN -I, -III, -V and -VI, laminin, fibulin -1, -4 and -7, fibrillin -1 and -2, filamin -A and -B, plectin, periostin, procollagen C-endopeptidase enhancer 1, the MMP inhibitor TIMP-1, and LOX-L1 and LOX-L2. The LOX enzymes are extracellular copper-dependent amine oxidases that catalyze the first step in the formation of crosslinking in collagens and elastin. LOX enzymes, TIMPs and MMPs alter the ECM, so FAP enzyme activity dependent changes in the relative abundance of any of those enzymes are very likely to cause FAP enzyme activity dependent indirect alterations of abundance or properties of many ECM proteins in CCM.

SILAC Applied to FAP e+ and FAP e− MEF Secretomes and Identification of Candidate FAP Substrates—TAILS highlighted that FAP activity had a pronounced impact on cell-contextual extracellular proteolysis. This finding prompted us to investigate effects of FAP activity on the composition of the MEF-derived cell conditioned medium (CCM) ("secretome"). For this purpose, we employed a QSTAR device, which was enough for medium proteome coverage. In data interpretation, we were particularly interested in the altered abundance of proteases and protease inhibitors. Differential quantitative proteomics used SILAC in five biological replicates (proteins listed in supplemental Tables S7–S11; peptides listed in supplemental Tables S12–S16).

TABLE I

37 bona fide FAP cleavage sites with P1 proline

Uniprot ID	Protein	Identified Peptide	P2	P1	Position	Protein length	Normalized log2 (FAP-active/ FAP-inactive)			mean log2 (FAP-active/ FAP-inactive)	S.D.	*P* Value
							Replicate 1	Replicate 2	Replicate 3			
P11087	Collagen alpha-1(I) chain;	MGPPGLAGPPGESGR	G	P	987	1453	4.46	7.58	7.25	6.43	1.71	0.001
		RGPPGPPGKNGDDGEAGKPGR PGER	G	P	207	1453	5.34	6.00		5.67	0.47	0.000
		AGAPGDKGEAGPSGPPGPTGAR	G	P	762	1453	1.48	3.00	2.86	2.44	0.84	0.003
		AGEKGSPGADGPAGSPGTPGP QGIAGQR	G	P	918	1453	3.17	NA	4.66	3.91	1.06	0.004
		SGLPGPPGER	G	P	465	1453	3.53	4.41	4.66	4.20	0.60	0.000
		SGNAGPPGPPGPVGKEGGKGPR	G	P	876	1453	NA	5.00	4.93	4.96	0.05	0.000
		IGNVGAPGPKGPR	G	P	840	1453	1.92	4.00	NA	2.96	1.47	0.018
		KGEPGSPGENGAPGQMGPR	G	P	273	1453	5.60	5.58	NA	5.59	0.01	0.000
		AGPPGPIGNVGAPGPKGPR	G	P	834	1453	9.84	6.58	7.25	7.89	1.72	0.000
		AGPIGPAGAR	G	P	1062	1453	3.83	1.03	2.20	2.35	1.41	0.016
		AGPAGPIGPAGAR	G	P	1059	1453	3.34	4.58	0.37	2.76	2.17	0.033
		AGPPGEAGKPGEQGVPGDLGAP GPSGAR	G	P	636	1453	3.60	6.00	5.66	5.09	1.30	0.001
		AGPAGPPGPIGNVGAPGPKGPR	G	P	831	1453	2.09	4.00	4.08	3.39	1.13	0.002
P08121	Collagen alpha-1(III) chain;	QGLPGQPGTAGEPGR	G	P	995	1464	2.71	NA	3.93	3.32	0.86	0.005
		AGFPGAPGQNGEPGAKGER	G	P	806	1464	NA	5.58	6.25	5.91	0.47	0.000
		GNDGKPGPPGSQGESGRPGPP GPSGPR	G	P	543	1464	NA	3.77	5.25	4.51	1.04	0.002
		AGPSGAPGPAGAR	G	P	1067	1464	4.46	6.00	NA	5.23	1.09	0.002
Q01149	Collagen alpha-2(I) chain;	MGLMGPR	G	P	97	177	NA	4.12	4.08	4.10	0.03	0.001
		AGEPGEPGQTGPAGPR	G	P	121	177	5.11	6.58	7.25	6.31	1.09	0.000
		SGIAGPPGPPGAAGKEGIR	G	P	805	1372	2.83	2.63	3.66	3.04	0.55	0.001
		SGKEGPVGLPGIDGRPGPIGPA GPR	G	P	466	1372	2.53	1.21	5.66	3.13	2.29	0.026
		SGAPGPDGNKGEAGAVGAPGSA GASGPGGLPGER	G	P	616	1372	1.56	6.58	4.66	4.27	2.53	0.012
		SGPNGPPGPVGSR	G	P	769	1372	0.61	3.49	3.79	2.63	1.76	0.021
		LGISGPPGAR	G	P	901	1372	2.25	3.06	2.49	2.60	0.41	0.001
		VGPPGNPGTNGLTGAKGATGLP GVAGAPGLPGPR	G	P	298	1372	4.92	4.41	1.63	3.66	1.77	0.006
		GAVGAPGPAGASGDR	I	P	683	1372	5.92	7.58	NA	6.75	1.17	0.001
		KDYEVDATLKSLNNQIETLLTPEGSR	R	P	1135	1372	NA	2.09	1.93	2.01	0.12	0.008
		AGSVGPVGAVGPR	G	P	988	1372	1.04	3.12	3.93	2.70	1.49	0.011
Q3U962	Collagen alpha-2(V) chain;	AGEPGKEGPPGLR	G	P	928	1497	3.22	3.67	NA	3.45	0.32	0.002
		TGFQGLPGPPGPPGEGGKAGDQ GVPGEPGAVGPLGPR	G	P	670	1497	3.28	6.58	NA	4.93	2.34	0.012
		VGPPGLAGER	G	P	652	1497	3.40	3.77	1.96	3.05	0.96	0.002
		EGPPGKPGEDGEPGR	G	P	253	1497	4.34	NA	3.55	3.94	0.56	0.002
Q6IR41	Complement C1q tumor necrosis factor-related protein 6; C1qT6	TEETTFGESVASHLPKGCR	V	P	25	264	NA	5.58	5.25	5.41	0.24	0.000
P50228	C-X-C motif chemokine 5; CXCL5	SSVIAATELR	A	P	41	132	0.80	0.83	0.59	0.74	0.13	0.040
D3YV64	Extracellular matrix protein 1; ECM-1	HTLAGQLPPEPR	K	P	142	251	NA	1.32	1.89	1.60	0.41	0.020
Q61555	Fibrillin-2;	EYRDEGAVAASR	G	P	60	2907	4.34	NA	7.25	5.79	2.06	0.005
P58022	Lysyl oxidase homolog 2; LOXL-2	EYFQQPAPEHHQR	Y	P	36	776	NA	1.35	1.89	1.62	0.38	0.019

As outlined for the TAILS approach, we employed limma statistics to delineate proteins that displayed significantly affected abundance in the presence of FAP enzyme activity. We chose the following criteria to distinguish significantly regulated proteins: (1) identification and quantitation in at least three replicate experiments, (2) annotation as a secreted or shed protein, (3) limma moderated p value < 0.05 and (4) average increase or decrease in abundance by more than 50% (log2 (FAP-active/FAP-inactive) > 0.58 for increase; log2 (FAP-active/FAP-inactive) < -0.58 for decrease). These criteria highlighted 31 more abundant and 33 less abundant proteins with increased FAP activity (limma statistics in supplemental Table S17).

Proteins That Were Differentially Abundant In the FAP e+ MEF secretome—Compared with FAP e−, the FAP e+ secretome contained more MMP-2 ("72 kDa type IV collagenase") and MMP-3 (Stromelysin-1). In addition to our initial interest in proteases and their inhibitors, we observed increased levels of CSF-1 and monocyte chemoattractant protein-1 (MCP-1/CCL-2) ($p_{limma} = 0.055$ - but increased in all 5 replicates and further considered because of its biological importance). This impact on CCL-2 is similarly observed in cancer associated fibroblasts (CAFs), where FAP activity leads to substantially elevated levels of CCL-2 (63).

Among proteins that were less abundant in the secretome of FAP e+ compared with FAP e− MEFs of particular interest were annexins A1 and A2 and the collagen - binding protease inhibitor serpin H1 (also seen with limma statistics on TAILS data; supplemental Table S5).

Validation of Candidate Substrates Found By TAILS—Selected candidate substrates identified through TAILS analysis were analyzed by *in vitro* cleavage assay. Recombinant proteins or synthetic N-terminal peptides corresponding to the secreted form of the protein were incubated with recombinant human FAP (rhFAP), and cleavage was then monitored over time by MALDI-TOF-MS analysis.

Secreted CXCL-5 (41–132) has Ala-Pro at the N terminus that TAILS identified as removed by FAP (Fig. 4*A*). *In vitro* cleavage using recombinant mouse CXCL-5 validated that observation. All the CXCL-5 lacked the Ala41-Pro42 after 24 h incubation with rhFAP (Fig. 4*B*). To examine a biological outcome of FAP-mediated cleavage in *ex vivo* physiological conditions, neutrophil migration assays were performed using CXCL-5 pre-incubated with FAP gki plasma, into which rhFAP or buffer (control) was added (Fig. 4*C*). The naturally occurring CXCL-5 in the FAP gki plasma increased neutrophil migration by 2-fold. Following FAP-mediated cleavage, the chemotactic activity of CXCL-5 was not altered (Fig. 4*C*).

C1qT6 is a 264 - residue protein of four domains and the secreted protein begins with a Val25-Pro26 sequence (Fig. 5*A*) that TAILS identified as removed by FAP. FAP-cleavage of C1qT6 was confirmed *in vitro* (Fig. 5*B*) using a synthetic peptide that represents the N-terminal 21 residues of secreted C1qT6 (25–45). Incubation with rhFAP yielded a cleavage product with a reduced mass of 218 Da within 5 min, with the mass shift corresponding to the removal of Val-Pro. The peptide was almost completely converted to 218 Da by 10 min (Fig. 5*B*), and within 30 min N-terminal processing of the C1qT6-derived peptide was complete (data not shown). This *in vitro* cleavage assay substantiates the enzymatic ability of FAP to process the N terminus of C1qT6.

The cleavage of LOX-L1 was observed at position 511 after a Lys-Ala sequence, with a $> 50\%$ average increase in abundance of the cleaved form ($p < 0.05$) (supplemental Table S5). Immunoblotting detected more LOX-L1 in the FAP e− than in the FAP e+ MEF CCM (Fig. 6). The whole cell lysates lacked this difference between the FAP e+ and e− MEFs (Fig. 6), consistent with the cleavage of LOX-L1 by FAP occurring extracellularly.

Confirming FAP Alters the MEF Secretome—The secretome analysis highlighted elevated levels of shed CSF-1 in the FAP e+ MEF secretome (supplemental Table S17). CSF-1 is important in the proliferation, differentiation, and survival of monocytes and macrophages. CSF-1 is a type I cell-surface protein that is released into the extracellular milieu by endoproteolytic shedding. We therefore probed cell-surface levels of CSF-1 using flow cytometry analysis and an antibody specific for the (potentially shed) N terminus of CSF-1 (Lys33-Glu262). That analysis showed 5-fold more cells immunopositive for CSF-1 in the FAP e− than in the FAP e+ MEF (Fig. 7*A*). Concordantly, immunoblotting on MEF cell lysates for CSF-1 showed that more cellular CSF-1 was in FAP e− than e+ MEFs (Fig. 7*B*). A possible explanation is that elevated shedding of CSF-1 in the FAP e+ MEFs leads to its depletion from the cell surface.

However, our data do not show that FAP directly acts as a CSF-1 sheddase. Although one TAILS experiment identified a P1-Pro, FAP-dependent cleavage site in CSF-1 in proximity to its annotated shedding site (Fig. 7*C*), FAP did not cut a synthetic peptide sequence that encompasses this sequence motif (Fig. 7*D*). Therefore, the impact of FAP on CSF-1 shedding is possibly indirect.

The present and previous proteomic studies strongly indicate that FAP activity results in increased levels of CCL-2 (63). Both human and mouse CCL-2 proteins have potential post-proline cleavage sites after Gln24-Pro25 and Ala30-Pro31. Full-length human and mouse CCL-2 were incubated with rhFAP and specific cleavage after Proline31 was shown by LC-MS/MS (Fig. 8*A*–8*C*). Monocyte migration assays assessed biological effects of this cleavage event. CCL-2 was able to induce monocyte migration. However, FAP, with or without the presence of a FAP specific inhibitor, did not alter the chemotactic activity of CCL-2 (Fig. 8*D*).

Candidate Substrates from Data Mining—Data mining and literature-based approaches were also utilized to search for candidate FAP substrates. FGF-21 was chosen as a candidate FAP endopeptidase substrate. Unlike most other candidate substrates, the cleavage site within FGF-21 is located

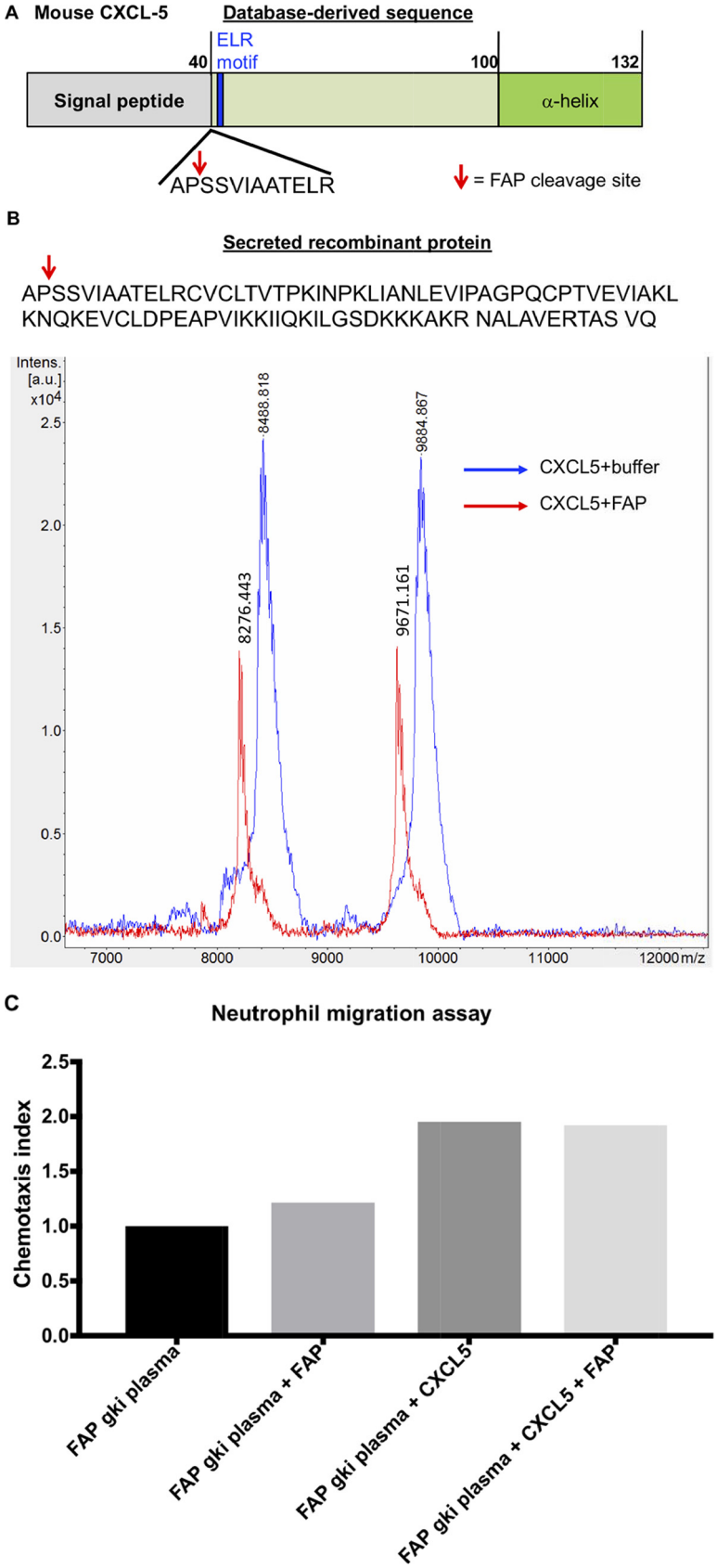
A
Mouse CXCL-5
Database-derived sequence
ELR
motif
40
100
132
Signal peptide
α-helix
APSSVIAATELR
= FAP cleavage site
B
Secreted recombinant protein
APSSVIAATELRCVCLTVTPKINPKLIANLEVIPAGPQCPTVEVIAKL
KNQKEVCLDPEAPVIKKIIQKILGSDKKKAKR NALAVERTAS VQ
Intens.
[a.u.]
x10^4
2.5
2.0
1.5
1.0
0.5
0.0
8488.818
9884.867
8276.443
9671.161
CXCL5+buffer
CXCL5+FAP
7000
8000
9000
10000
11000
12000 m/z
C
Neutrophil migration assay
Chemotaxis index
2.5
2.0
1.5
1.0
0.5
0.0
FAP gki plasma
FAP gki plasma + FAP
FAP gki plasma + CXCL5
FAP gki plasma + CXCL5 + FAP

within a dozen residues of the C- rather than N terminus (Fig. 9*A*). Recombinant human FGF-21 (hFGF-21) matching residues 29–209 (lacking the signal peptide) was analyzed in MALDI-TOF-MS and LC-MS/MS analyses to investigate whether this protein undergoes FAP cleavage. By MALDI, the doubly charged ion was identified (peak at ~9785 Da) and after 10 min incubation with FAP a smaller peak corresponding to hFGF-21 lacking the last 10 amino acids (~9296 Da) was observed, and after 2 h incubation hFGF-21 was completely digested by FAP (Fig. 9*B*). No cleavage was observed in the absence of FAP (data no shown). To confirm hFGF-21 as a FAP substrate *in vitro*, LC-MS/MS analysis was performed using the enzyme AspN rather than trypsin. Only AspN-cleaved peptides were identified in the control. In the FAP-treated sample the peptide C-terminal to the cleavage site was identified but the peptide N-terminal to this cleavage site was not detected. However, 33.7% sequence coverage of FGF-21 was observed in the untreated sample, whereas only 5.5% sequence coverage was observed in the FAP-treated sample. Taken together, the LC-MS/MS data and MALDI-TOF-MS data demonstrated that hFGF-21 undergoes *in vitro* cleavage by FAP after proline 171 (Fig. 9*C*).

Influence of FAP on Coagulation—The present work highlights a strong impact of FAP on extracellular proteolysis (both directly and indirectly). Cleavage of human α2-antiplasmin by FAP has implicated the activity of FAP in fibrinolysis (14). In the present study, FAP affected the proteolytic processing of several mouse proteins with functions in coagulation, such as prothrombin and thrombospondin-2 (supplemental Table S5), indicating that FAP might influence coagulation. Therefore, plasma was isolated from WT and FAP GKO mice and prothrombin times (PT) and activated partial thromboplastin times (APTT) were measured. PT examines the extrinsic coagulation pathway, whereas APTT test examines the intrinsic coagulation pathway. No significant difference in prothrombin times between WT and FAP GKO mouse plasma was observed (Fig. 10*A*). However, a significant increase in activated partial prothrombin times was observed in the FAP GKO plasma compared with WT plasma ($p = 0.033$; Fig. 10*B*).

Full blood counts on WT and FAP GKO mice showed no difference in platelet numbers or any other major blood cell type (supplemental Table S18), which is consistent with the initial description of this mouse strain (24, 65).

DISCUSSION

A large number of FAP-driven cleavage events were identified using TAILS. A strength of the approach taken was the production of a cellular source of substrates, from GKO MEFs, that had never been exposed to FAP or its enzyme activity. Many of the detected cleavage events are likely to be direct cleavage by FAP, whereas others may be caused indirectly. Global differential proteomics showed differential abundance of several proteases and protease inhibitors that probably contributed indirect cleavage events to our data.

Much of the detected post-proline cleavage by FAP was of collagens and other ECM proteins, including CN-I, CN-III, CN-V, fibrillin-2 and ECM-1 (Table I). Fibroblasts are the main cellular source of ECM proteins, so it is sensible that many ECM proteins were detected in CCM from MEFs. Nevertheless, the preponderance of ECM associated candidate substrates was the dominant finding of this study.

In addition, many proteolytic events were observed in a range of ECM proteins that did not correspond to post-proline processing, suggesting either that FAP is not restricted to cleavage after a proline and/or that FAP drives increased levels of other ECM - degrading proteases. The many ECM associated proteins identified as differentially abundant include collagens, laminins, fibronectin, periostin, cofilin-1, cathepsin-B, fibrillin-1, fibulin-1, ECM-1, serpin-H1, LOX-L1, NCAM-1 and the ECM degrading enzymes MMP-2 and MMP-3 and MMP inhibitors TIMP-1 and TIMP-2, in the FAP e+ or FAP e− secretome (supplemental Table S17). These data may point to a FAP-MMP-TIMP axis of ECM regulation. The lysyl oxidases are of particular interest because they drive collagen crosslinking (66), which is crucial in liver fibrosis (67). In addition to directly causing degradation of LOX-L1 (Fig. 5), we saw that FAP altered the levels of BMP-1 and periostin (supplemental Table S17), which can promote LOX activation (68). Considered together, the data suggests that when FAP e+ is expressed it results in greater levels of ECM proteolysis, ECM degrading enzymes and their inhibitors and other ECM associated proteins, which points to a significant role for FAP in the regulation of ECM degradation. These insights are consistent with the known importance of FAP in ECM-dependent cancer cell and fibroblast invasion and migration (28, 69–72) and more generally in cell - ECM interactions (4, 12, 73, 74). Annexin A2 is involved in fibrinolysis (75), and has been shown to interact with FAP (76, 77). Several proteins found to be cut or differentially abundant in the presence of FAP enzyme activity are important in liver fibrosis, including CYR-61 (CCN-1) (78, 79), and in iron storage, including ferritins and lipocalin (LCN2) (80). These data, together with a recent study (63), highlight that differential FAP activity has a profound effect on the secretome, hence characterizing FAP as a key player in shaping the pericellular environment.

Post-translational modifications (PTM) modify proteins including interaction between a substrate and an enzyme. Although synthetic proteins or peptides may not possess PTM

FIG. 4. **In vitro examination of candidate substrate CXCL-5.** *A*, Schematic of the genome - encoded primary structure of mouse CXCL-5. The Uniprot-annotated N-terminal sequence is shown with the proposed FAP cleavage site indicated by a red arrow after Pro42. *B*, MALDI-TOF-MS spectra showing removal of Ala-Pro from the N terminus of mCXCL-5. *C*, Neutrophil migration assay using mCXCL-5 pre-incubated with FAPgki plasma, with rhFAP or buffer (control), at 37 °C for 24 h. Data are representative of two independent experiments.

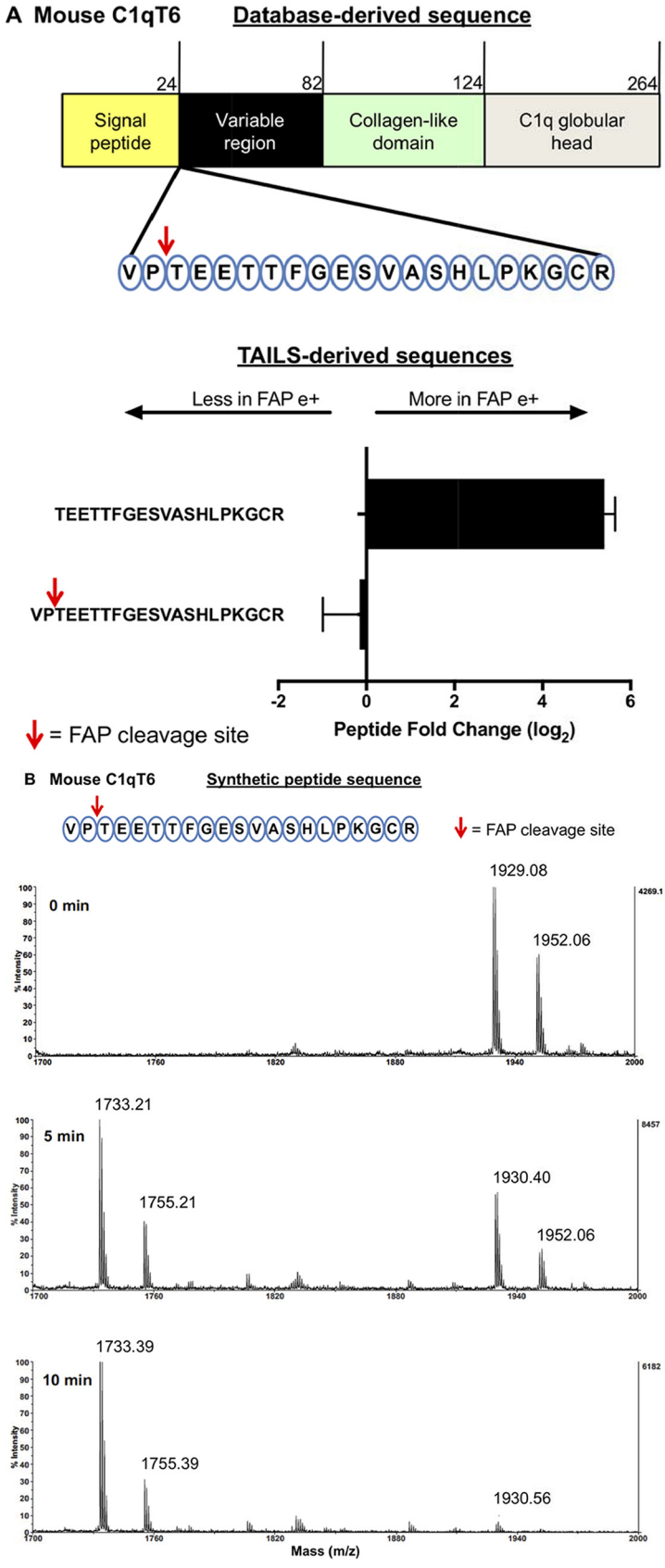
A Mouse C1qT6
Database-derived sequence
24
82
124
264
Signal peptide
Variable region
Collagen-like domain
C1q globular head
V P T E E T T F G E S V A S H L P K G C R
TAILS-derived sequences
Less in FAP e+
More in FAP e+
TEETTFGESVASHLPKGCR
VPTEETTFGESVASHLPKGCR
-2
0
2
4
6
= FAP cleavage site
Peptide Fold Change (log2)
B Mouse C1qT6
Synthetic peptide sequence
V P T E E T T F G E S V A S H L P K G C R
= FAP cleavage site
0 min
1929.08
1952.06
4269.1
5 min
1733.21
1755.21
1930.40
1952.06
8457
10 min
1733.39
1755.39
1930.56
6182
% Intensity
Mass (m/z)

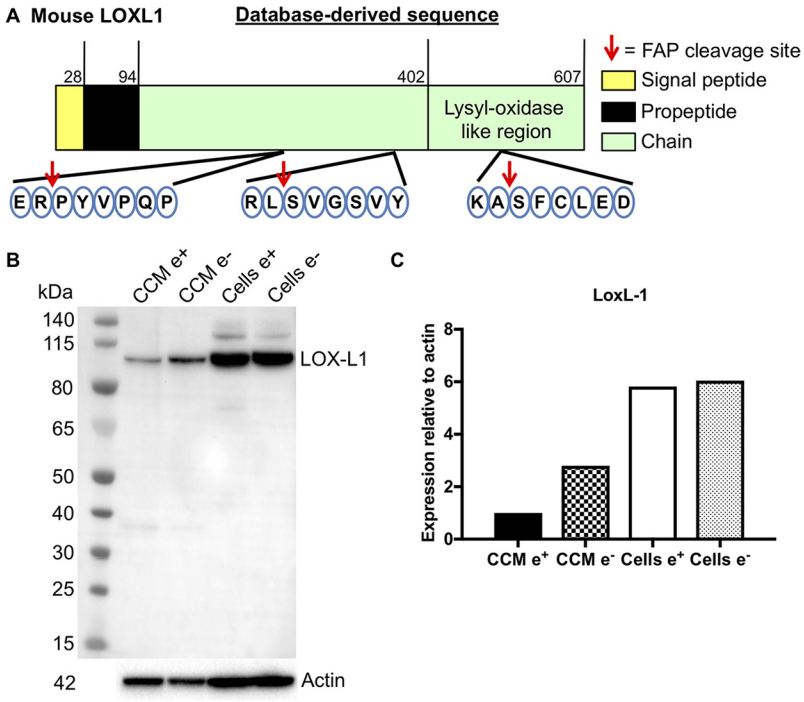

FIG. 6. **In vitro examination of candidate substrate LOX-L1.** *A*, Schematic of the primary structure of mouse LOX-L1. The Uniprot-annotated protein sequence is shown with the proposed FAP cleavage site indicated by red arrows. *B*, LOX-L1 immunoblotting of whole cell lysates and of cell conditioned medium (CCM) from the FAP e+ and e− MEFs. *C*, Densitometry was performed using beta-actin as loading control. The data are representative of three independent experiments.

that occur *in vivo*, they are often useful for initial substrate validation. Mouse CXCL-5 contains a DPP substrate cleavage site at Ala-Pro at the N terminus after the signal peptide is removed. The secreted form of mCXCL-5 has 92 amino acids (41–132) and can be further cleaved into two isoforms that have 78 residues (41–118) and 70 residues (49–118) respectively. These truncated isoforms are more potent than the secreted CXCL-5 (41–132) at inducing neutrophil infiltration *in vitro* (81). Because the FAP cleavage site is quite close to the ELR motif that is important for receptor binding, FAP-truncated CXCL-5 might show enhanced chemotactic activity as well. However, neutrophil chemotaxis was not different between intact and FAP-truncated CXCL-5. Thus, dipeptide removal from the N terminus of CXCL-5 does not affect the biological potency of this chemokine.

C1qT6 is a clear candidate substrate, with the mature N terminus present in the FAP e− secretome and the protease-generated neo-N terminus in the FAP e+ secretome (Fig. 4). C1qT6 is a member of the C1q/TNF-related protein (CTRP) family, which contains adiponectin (82). C1qT6 also has roles in coagulation and arthritis (83), possibly hepatocellular carcinoma (84), and metabolic disorders (85). Although removal of just two N-terminal amino acids might not have a significant effect on C1qT6, because the known biological function of this protein is induced via its C-terminal domain (86), DPP cleavage of C1qT6 might confer upon this protein increased susceptibility to further digestion by other proteases, leading to production of the naturally occurring truncated form.

The *in vitro* endopeptidase cleavage by FAP of both human and mouse CCL-2 (Fig. 7) is the first report of a natural FAP endopeptidase substrate being cleaved after an alanine-proline sequence. CCL-2 has ubiquitous pro-inflammatory actions (70, 87, 88) through binding to its cognate receptor CCR2. Removing the first 8 amino acids off the N terminus of CCL-2 converts it into a receptor antagonist that retains the ability to bind to CCR2 but not the ability to elicit a chemotactic response (87, 89). Therefore, a truncated CCL-2 analog has been developed as an anti-inflammatory therapeutic (90, 91). The cleavage of CCL-2 by FAP, resulting in the removal of the first 8 amino acids, would convert it into a dominant negative receptor antagonist. However, chemotaxis ability of

FIG. 5. **In vitro examination of candidate substrate C1qT6.** *A*, Schematic of the primary structure of mouse C1qT6. The Uniprot-annotated N terminus sequence is shown with proposed FAP cleavage site indicated by a red arrow after Pro26. The peptide identified from TAILS analysis and the corresponding fold changes are shown. Mean ± S.D.; $n = 2–3$. *B*, MALDI-TOF-MS spectra showing removal of Val-Pro dipeptide from the N terminus of synthetic recombinant peptide, consistent with a peak shift of 203. The peptide was almost completely cleaved at 10 min. The synthetic peptide had two forms, which differed in mass by ~22 daltons as indicated by the presence of two peaks. Both forms were hydrolyzed by FAP.

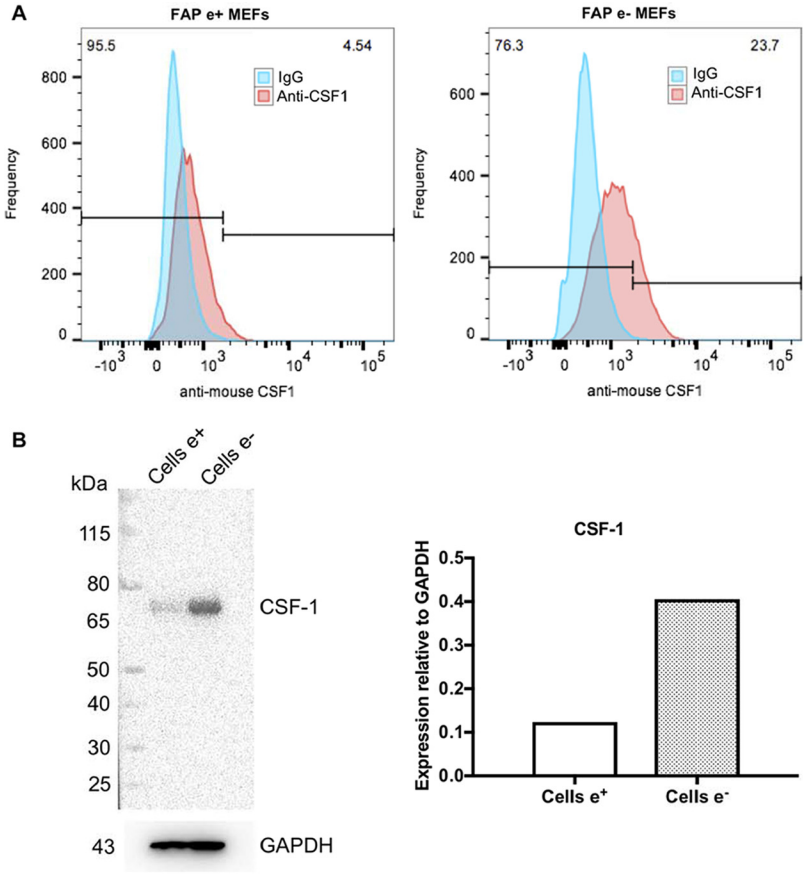

FIG. 7. **In vitro examination of candidate substrate CSF-1.** *A*, CSF-1 primary antibody paired with a secondary anti-goat Alexa Fluor 647 stained the N terminus of CSF-1 in the FAP e+ and e− MEFs after permeabilization with 0.05% (w/v) saponin. 23.7% of FAP e− MEFs were immunopositive compared with only 4.5% of the FAP e+ MEFs. Goat IgG was used as a negative control. *B*, Immunoblotting of CSF-1 in whole cell lysates revealed more cellular CSF-1 present in FAP e− MEFs than FAP e+ MEFs. Densitometry was performed using GAPDH as a loading control. (*A*, *B*) Representative of two independent experiments. *C*, Schematic of the primary structure of CSF-1. The Uniprot-annotated N terminus sequence is shown with the proposed FAP cleavage site indicated by a red arrow after Pro449. This cleavage site identified in TAILS is in the extracellular region, near the transmembrane domain. Identified peptide from TAILS analysis and its corresponding fold change are shown. Synthetic recombinant peptide consists of Ser442 to Arg463, with the proposed FAP cleavage site indicated by a red arrow. *D*, MALDI-TOF-MS showing no cleavage of the synthetic recombinant CSF-1 peptide after 16 h incubation with rhFAP at 37 °C.

intact or FAP-cleaved CCL-2 in monocytes was not changed, indicating that FAP derived cleavage of CCL-2 does not regulate the bioactivity of this chemokine.

Recently, FGF-21 cleavage by FAP has been reported (8–10). Such cleavage was also observed here, by LC-MS/MS coupled with MALDI-TOF-MS, showing that human FGF-21 undergoes cleavage by FAP after Pro171 *in vitro* (Fig. 9). Administering a selective FAP inhibitor acutely increases circulating intact FGF-21 levels in cynomolgus monkeys (8) and prolongs the half-life of circulating human FGF-21 in mice (10), therefore FGF-21 is a physiological substrate for FAP. Proteins that were identified by TAILS and have roles in lipid or energy metabolism include proprotein convertase subtilisin/kexin type 9 (PCSK-9), pyruvate kinase PKM, insulin-2, PYY, clusterin (apolipoprotein J) and low-density lipoprotein receptor 8 (LRP-8) (supplemental Table S5). Thus, FAP may have important influences on energy metabolism.

FAP has a well-established role in clotting and fibrinolysis in humans and this role is mediated by cleavage of α2-antiplasmin (11, 14), but other FAP-interacting molecules might be involved (77). Mouse α2-antiplasmin lacks the FAP cleavage site and a role for FAP in clotting in the mouse had not been reported. However, our degradomics and proteomics data pointed to the potential for a role for FAP in coagulation in the mouse. Concordantly, we observed that, as in humans (14), depletion of FAP from plasma slows the clotting time in mice (Fig. 10). The proteins that we identified as potentially mediating this physiological outcome are FSTL-1 (92), C1qT6 (83), SNED-1, filamin-A, serpin-G1, thrombospondin-1, thrombospondin-2, and PAI-1 (supplemental Tables S5 and S17). Our finding that mouse plasma that lacks FAP exhibited slowed coagulation is consistent with the identification of a number of potential FAP substrates that are coagulation - associated.

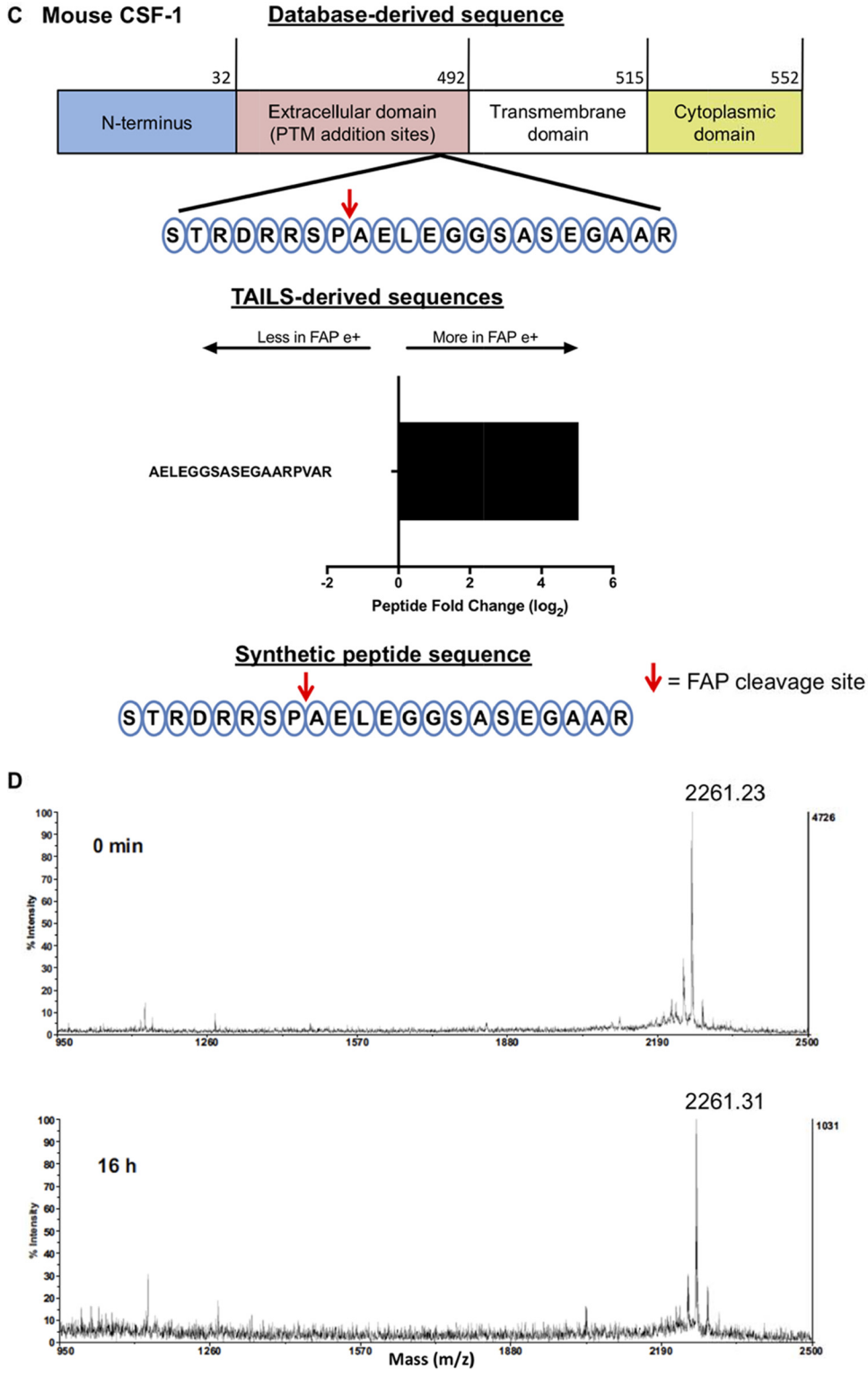

FIG. 7—*continued*

CONCLUSION

This study focused on identifying novel substrates of FAP and the downstream effects of FAP enzyme activity on the MEF secretome. Many potential FAP substrates were identified, including many ECM and immunoregulatory proteins, and several were confirmed that may have implications for the role of FAP in health and disease. Future investigations into which natural substrates are indirectly cleaved, via other en-

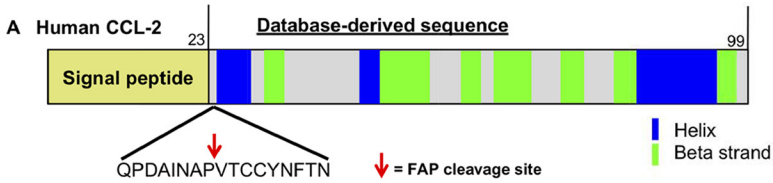

B Human CCL-2 **Secreted recombinant protein**

QPDAINAPVTCCYNFTNRKISVQRLASYRRITSSKCPKE
AVIFKTIVAKEICADPKQKWVQDSMDHLDKQTQTPKT

LC-MS/MS-derived sequences

no FAP	+ FAP
QPDAINAPVTCCYNFTNR	QPDAINAPVTCCYNFTNR
QPDAINAPVTCCYNFTNRK	QPDAINAPVTCCYNFTNRK
	VTCCYNFTNRK
ISVQRLASYR*	ISVQRLASYR*
ITSSKCPK*	ITSSKCPK*
CPKEAVIFK*	CPKEAVIFK*
EAVIFKTIVAK*	EAVIFKTIVAK*
TIVAKEICADPK*	TIVAKEICADPK*
EICADPKQK*	EICADPKQK*
QKWVQDSMDHLDK*	QKWVQDSMDHLDK*
WVQDSMDHLDK	WVQDSMDHLDK
WVQDSMDHLDKQTQTPK*	WVQDSMDHLDKQTQTPK*
QTQTPKT*	QTQTPKT*

C Mouse CCL-2 **Secreted recombinant protein** = FAP cleavage site

QPDAVNAPLTCCYSFTSKMIPMSRLESYKRITSSRCPKEAVVFV
TKLKREVCADPKKEWVQTYIKNLDRNQMRSEPTTLFKTASALR
SSAPLNVKLTRKSEANASTTFSTTTSSTSVGVTSVTVN

LC-MS/MS-derived sequences

no FAP	+ FAP
QPDAVNAPLTCCYSFTSK	QPDAVNAPLTCCYSFTSK
	LTCCYSFTSK

*LC-MS/MS identified peptide contains a missed AspN cleavage

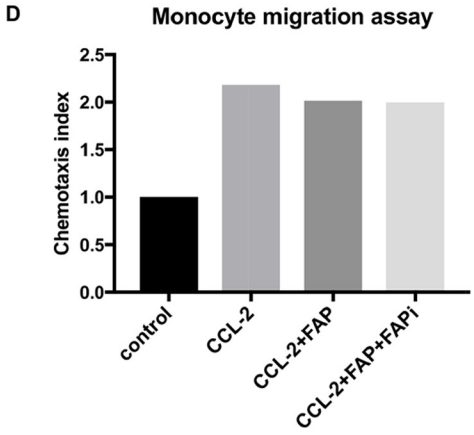

FIG. 8. **In vitro examination of candidate substrate human CCL-2 (hCCL-2) and mouse CCL-2 (mCCL-2) using LC-MS/MS.** *A*, Schematic of the primary structure of hCCL-2. The Uniprot-annotated N terminus sequence is shown with the proposed FAP cleavage site indicated by a red arrow after Pro31. *B*, *C*, Database-derived amino acid sequences of recombinant hCCL-2 (*B*) and mCCL-2 (*C*) are shown with red arrows indicating the FAP cleavage sites. The peptide sequence that is colored red corresponds to a peptide produced by FAP-mediated cleavage. Black and gray alternating peptides represent the peptides potentially produced by digestion with trypsin. Recombinant hCCL-2 and mCCL-2 were incubated with rhFAP (+ FAP) or a buffer control (no FAP) for 4 h at 37 °C. Samples were then treated with trypsin and analyzed by LC-MS/MS. 98% sequence coverage of hCCL-2 was observed in both samples, whereas 14% sequence coverage of mCCL-2 was seen, and the truncated peptides matching to the FAP-cleavage products were identified only in the samples that had been treated with FAP. Some trypsin cleavages were missed (*). Representative data from two technical replicates. *D*, Monocyte migration assay using mCCL-2 pre-incubated at 37 °C for 24 h with buffer (control), rhFAP, or rhFAP with a specific FAP inhibitor (FAPi). Data are representative of two independent experiments.

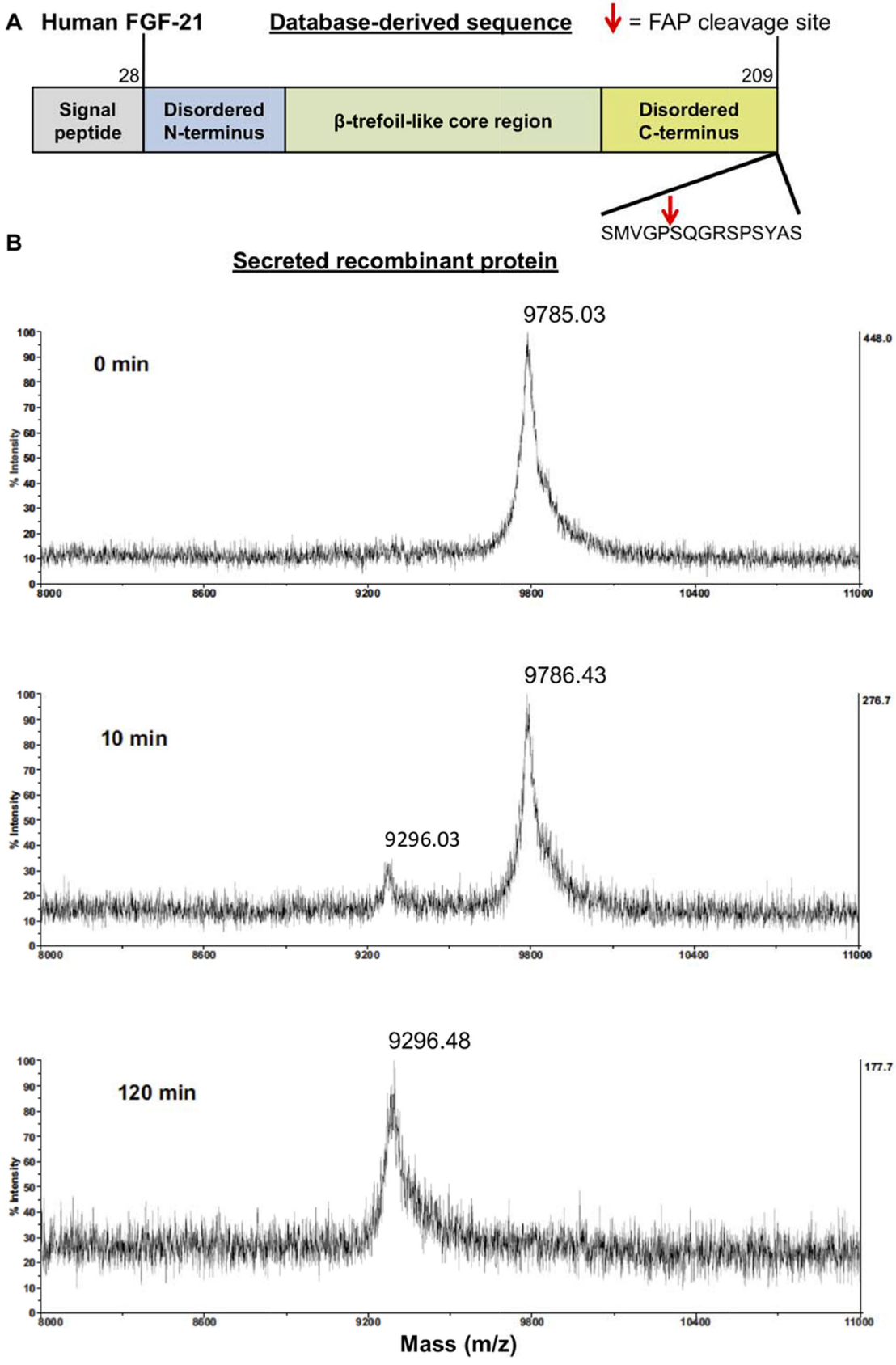
A Human FGF-21
Database-derived sequence
= FAP cleavage site
28
209
Signal peptide
Disordered N-terminus
β-trefoil-like core region
Disordered C-terminus
SMVGPSQGRSPSYAS
B
Secreted recombinant protein
9785.03
0 min
448.0
9786.43
10 min
276.7
9296.03
9296.48
120 min
177.7
% Intensity
Mass (m/z)

C Human FGF-21 Secreted recombinant protein ↓ = FAP cleavage site

MHPIPDSSPLLQFGGQVRQRYLYTDDAQQTEAHLEIREDGTVGGAADQSPESL
LQLKALKPGVIQILGVKTSRFLCQRPDGALYGSLHFDPEACSFRELLLEDGYNV
YQSEAHGLPLHLPGNKSPHRDPAPRGPARFLPLPGLPPALPEPPGILAPQPPD
VGSSDPLSMVGPSQGRSPSYAS

LC-MS/MS-derived sequences

no FAP	+ FAP
DSSPLLQFGGQVRQRYLYT	SQGRSPSYAS
DDAQQTEAHLEIRE*	
DDAQQTEAHLEIREDGTVGGAA*	
DGYNVYQSEAHGLPLHLPGNKSPHR	
DPAPRGPARFLPLPGLPPALPEPPGILAPQPP	
DVGSSDPLSMVGPAQGRSPSYAS*	

*LC-MS/MS identified peptide contains a missed AspN cleavage

FIG. 9—*continued*

zymes, rather than by direct FAP-mediated cleavage, may provide greater understanding of the pathogenesis of tumors and of fibrotic disorders.

Acknowledgments—We thank Geoffrey Kershaw of Hematology Department, Royal Prince Alfred Hospital for coagulation assays, veterinary pathology diagnostic services of The University of Sydney for blood cell counts, Emaleen Najjar for assistance with some immunoblots and cell culture, Dr Ben Crossett of Mass Spectrometry Core Facility, The University of Sydney, for assistance with MALDI-TOF-MS, and Franz Jehle for mass spectrometry technical support. We thank Dr William W. Bachovchin for kindly providing Val-boro-Pro and ARI-3099 and Dr Andreas Schnapp for the FAP GKO mouse strain.

DATA AVAILABILITY

The mass spectrometry proteomics data (pep-XML files, .raw/.wiff files, mzXML files) have been deposited to the ProteomeXchange Consortium (53) via the PRIDE partner repository with the data set identifiers PXD004754 and PXD004757. Annotated spectra of the TAILS data and of the global quantitative proteome comparison are provided at MS-viewer (54). The experiments and the corresponding Search Keys are listed in supplemental Table S1.

* This work was supported by project grant 1105238 from the Australian National Health and Medical Research Council (MDG, GWM, SMT) and grants from the Rebecca L. Cooper Medical Research Foundation (MDG) and an Australian Postgraduate Award (EJH). MDG and OS were supported by a grant from the Group of Eight Australia - Deutscher Akademischer Austauschdienst Joint Research Co-operation Scheme. OS acknowledges support by Deutsche Forschungsgemeinschaft (GR 1748/6-1, SCHI 871/8-1, SCHI 871/9-1, SCHI 871/11-1, SCHI 871/12-1, INST 39/900-1, and SFB850-Project Z1 (INST 39/766-3)), the Excellence Initiative of the German Federal and State Governments (EXC 294, BIOSS), and the Germany-Israel Foundation (Grant No. I-1444-201.2/2017).

S This article contains supplemental material. The authors declare no competing interests.

|||| To whom correspondence may be addressed: Liver Enzymes in Metabolism and Inflammation Program, Centenary Institute, Locked Bag No. 6, Newtown, NSW. E-mail: m.gorrell@centenary.usyd.edu.au.

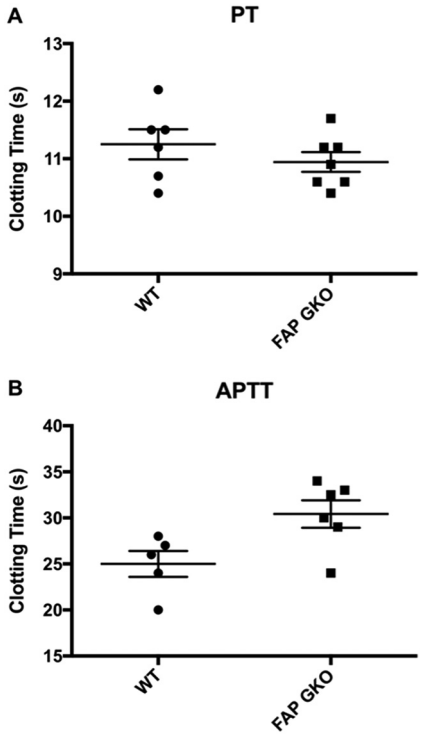

FIG. 10. **Influence of FAP on the extrinsic and intrinsic coagulation pathways.** Plasma was collected from wild type (WT) and FAP gene knockout (GKO) mice and prothrombin times (PT) and activated partial thromboplastin times (aPTT) were measured. *A*, No significant difference in prothrombin times between WT and FAP GKO mouse plasma was observed. *B*, A significant increase in activated partial prothrombin times was observed in the FAP GKO plasma compared with WT plasma ($p = 0.0325$). Mean ± S.E., $n = 5–7$.

FIG. 9. ***In vitro* examination of candidate substrate human FGF21 (hFGF21).** *A*, Schematic of the primary structure of hFGF21. The Uniprot-annotated N terminus sequence is shown with proposed FAP cleavage site indicated by a red arrow after Pro199. *B*, MALDI-TOF-MS spectra showing cleavage after Gly-Pro199. The ~9786 Da peak corresponds to the doubly charged full-length protein. After 10 min incubation with rhFAP at 37 °C, cleavage resulted in the ~9296 Da peak corresponding to the full-length protein lacking the last 10 amino acids. FGF-21 was fully digested at 120 min incubation with rhFAP. *C*, Database-derived amino acid sequence of rhFGF21, with a red arrow at the FAP cleavage site and the red peptide corresponds to the peptide produced from FAP cleavage. Black and gray alternating peptides represent the peptides produced after digestion with AspN. Recombinant hFGF21 was incubated with rhFAP (+ FAP) or a buffer control (no FAP) for 30 min at 37 °C, digested with AspN and analyzed by LC-MS/MS. The peptides identified in each sample are listed; 33.7% sequence coverage of rhFGF21 was observed in the untreated sample whereas only 5.5% sequence coverage was observed in the rhFAP-treated sample, and the truncated peptide matching to the FAP-cleavage product was identified only in the sample that was treated with rhFAP. Representative of two technical replicates.

¶¶¶ To whom correspondence may be addressed: Institute of Surgical Pathology, University Medical Center – University of Freiburg, Breisacher Str. 115A, 79106, Freiburg, Germany. E-mail: oliver.schilling@mol-med.uni-freiburg.de.

‡‡‡ Equal first authors.

§§§ Equal senior authors.

Author contributions: H.E.Z., E.J.H., S.T., S.C., C.G.B., M.M.K., A.J.L., Q.L., B.R., M.L.B., M.O., F.M.K., and O.S. performed research; H.E.Z., E.J.H., S.T., S.C., M.M.K., A.J.L., S.M.T., Q.L., B.R., M.L.B., M.O., F.M.K., O.S., and M.D.G. analyzed data; H.E.Z., E.J.H., S.M.T., G.W.M., F.M.K., O.S., and M.D.G. wrote the paper; E.J.H., C.G.B., Q.L., B.R., G.W.M., F.M.K., O.S., and M.D.G. designed research; S.T., C.G.B., Q.L., and O.S. contributed new reagents/analytic tools.

REFERENCES

1. Park, J. E., Lenter, M. C., Zimmermann, R. N., Garin-Chesa, P., Old, L. J., and Rettig, W. J. (1999) Fibroblast activation protein: A dual-specificity serine protease expressed in reactive human tumor stromal fibroblasts. *J. Biol. Chem.* **274,** 36505–36512
2. Aertgeerts, K., Levin, I., Shi, L., Snell, G. P., Jennings, A., Prasad, G. S., Zhang, Y., Kraus, M. L., Salakian, S., Sridhar, V., Wijnands, R., and Tennant, M. G. (2005) Structural and kinetic analysis of the substrate specificity of human fibroblast activation protein {alpha}. *J. Biol. Chem.* **280,** 19441–19444
3. Lee, K. N., Jackson, K. W., Christiansen, V. J., Lee, C. S., Chun, J. G., and McKee, P. A. (2006) Antiplasmin-cleaving enzyme is a soluble form of fibroblast activation protein. *Blood* **107,** 1397–1404
4. Hamson, E. J., Keane, F. M., Tholen, S., Schilling, O., and Gorrell, M. D. (2014) Understanding Fibroblast Activation Protein (FAP): substrates, activities, expression and targeting for cancer therapy. *Proteomics Clin. Appl.* **8,** 454–463
5. Polak, N., and Gorrell, M. D. (2018) Fibroblast activation protein; FAP. In: Choi, S., ed. *Encyclopedia of Signaling Molecules*, 2nd Ed., pp. 1676–1681, Springer International Publishing, Cham
6. Juillerat-Jeanneret, L., Tafelmeyer, P., and Golshayan, D. (2017) Fibroblast activation protein-alpha in fibrogenic disorders and cancer: more than a prolyl-specific peptidase? *Expert Opin. Ther. Targets* **21,** 977–991
7. Keane, F. M., Nadvi, N. A., Yao, T.-W., and Gorrell, M. D. (2011) Neuropeptide Y, B-type natriuretic peptide, substance P and peptide YY are novel substrates of fibroblast activation protein-α. *FEBS J.* **278,** 1316–1332
8. Dunshee, D. R., Bainbridge, T. W., Kljavin, N. M., Zavala-Solorio, J., Schroeder, A. C., Chan, R., Corpuz, R., Wong, M., Zhou, W., Deshmukh, G., Ly, J., Sutherlin, D. P., Ernst, J. A., and Sonoda, J. (2016) Fibroblast activation protein cleaves and inactivates fibroblast growth factor 21. *J. Biol. Chem.* **291,** 5986–5996
9. Zhen, E. Y., Jin, Z., Ackermann, B. L., Thomas, M. K., and Gutierrez, J. A. (2016) Circulating FGF21 proteolytic processing mediated by fibroblast activation protein. *Biochem. J.* **473,** 605–614
10. Coppage, A. L., Heard, K. R., DiMare, M. T., Liu, Y., Wu, W., Lai, J. H., and Bachovchin, W. W. (2016) Human FGF-21 is a substrate of fibroblast activation protein. *PLoS ONE* **11**, e0151269
11. Lee, K. N., Jackson, K. W., Christiansen, V. J., Chung, K. H., and McKee, P. A. (2004) A novel plasma proteinase potentiates alpha2-antiplasmin inhibition of fibrin digestion. *Blood* **103,** 3783–3788
12. Christiansen, V. J., Jackson, K. W., Lee, K. N., and McKee, P. A. (2007) Effect of fibroblast activation protein and alpha2-antiplasmin cleaving enzyme on collagen types I, III, and IV. Arch. Biochem. *Biophys.* **457,** 177–186
13. Wong, P. F., Gall, M. G., Bachovchin, W. W., McCaughan, G. W., Keane, F. M., and Gorrell, M. D. (2016) Neuropeptide Y is a physiological substrate of fibroblast activation protein: Enzyme kinetics in blood plasma and expression of Y2R and Y5R in human liver cirrhosis and hepatocellular carcinoma. *Peptides* **75,** 80–95
14. Lee, K. N., Jackson, K. W., Christiansen, V. J., Dolence, E. K., and McKee, P. A. (2011) Enhancement of fibrinolysis by inhibiting enzymatic cleavage of precursor alpha2-antiplasmin. *J. Thromb Haemost.* **9,** 987–996
15. Sánchez-Garrido, M. A., Habegger, K. M., Clemmensen, C., Holleman, C., Müller, T. D., Perez-Tilve, D., Li, P., Agrawal, A. S., Finan, B., Drucker, D. J., Tschöp, M. H., DiMarchi, R. D., and Kharitonenkov, A. (2016) Fibroblast activation protein (FAP) as a novel metabolic target. *Mol. Metabolism* **5,** 1015–1024
16. Lo, A., Li, C.-P., Buza, E. L., Blomberg, R., Govindaraju, P., Avery, D., Monslow, J., Hsiao, M., and Puré, E. (2017) Fibroblast activation protein augments progression and metastasis of pancreatic ductal adenocarcinoma. *JCI Insight* **2**, pii: 92232
17. Gerhard, G. S., Legendre, C., Still, C. D., Chu, X., Petrick, A., and DiStefano, J. K. (2018) Transcriptomic profiling of obesity-related nonalcoholic steatohepatitis reveals a core set of fibrosis-specific genes. *J. Endocrine Soc.* **2,** 710–726
18. Huang, S. C., Fang, R., Xu, J., Qiu, S. H., Zhang, H., Du, J., and Cai, S. H. (2011) Evaluation of the tumor targeting of a FAP alpha-based doxorubicin prodrug. *J. Drug Target.* **19,** 487–496
19. Tinoco, A. D., Tagore, D. M., and Saghatelian, A. (2010) Expanding the Dipeptidyl Peptidase 4-Regulated Peptidome via an Optimized Peptidomics Platform. *J. Am. Chem. Soc.* **132,** 3819–3830
20. Wilson, C. H., Indarto, D., Doucet, A., Pogson, L. D., Pitman, M. R., Menz, R. I., McNicholas, K., Overall, C. M., and Abbott, C. A. (2013) Identifying natural substrates for dipeptidyl peptidase 8 (DP8) and DP9 using terminal amine isotopic labelling of substrates, TAILS, reveals in vivo roles in cellular homeostasis and energy metabolism. *J. Biol. Chem.* **288,** 13936–13949
21. Zhang, H., Maqsudi, S., Rainczuk, A., Duffield, N., Lawrence, J., Keane, F. M., Justa-Schuch, D., Geiss-Friedlander, R., Gorrell, M. D., and Stephens, A. N. (2015) Identification of novel dipeptidyl peptidase 9 substrates by two-dimensional differential in-gel electrophoresis. *FEBS J.* **282,** 3737–3757
22. Wilson, C. H., Zhang, H. E., Gorrell, M. D., and Abbott, C. A. (2016) Dipeptidyl peptidase substrate discovery: Current progress and the application of mass spectrometry - based approaches. *Biol. Chem.* **397,** 837–856
23. Ritchie, M. E., Phipson, B., Wu, D., Hu, Y., Law, C. W., Shi, W., and Smyth, G. K. (2015) limma powers differential expression analyses for RNA-sequencing and microarray studies. *Nucleic Acids Res.* **43,** e47
24. Niedermeyer, J., Kriz, M., Hilberg, F., Garin-Chesa, P., Bamberger, U., Lenter, M. C., Park, J., Viertel, B., Puschner, H., Mauz, M., Rettig, W. J., and Schnapp, A. (2000) Targeted disruption of mouse fibroblast activation protein. *Mol. Cell. Biol.* **20,** 1089–1094
25. Niedermeyer, J., Enenkel, B., Park, J. E., Lenter, M., Rettig, W. J., Damm, K., and Schnapp, A. (1998) Mouse fibroblast-activation protein: Conserved *Fap* gene organization and biochemical function as a serine protease. *Eur. J. Biochem.* **254,** 650–654
26. Gall, M. G., Chen, Y., Ribeiro A. J. V. d., Zhang, H., Bailey, C. G., Spielman, D., Yu, D. M., and Gorrell, M. D. (2013) Targeted inactivation of Dipeptidyl Peptidase 9 enzyme activity causes mouse neonate lethality. *PLoS ONE* **8**, e0078378
27. Guan, F. H. X., Bailey, C. G., Metierre, C., O'Young, P., Gao, D., Khoo, T. L., Holst, J., and Rasko, J. E. J. (2017) The antiproliferative ELF2 isoform, ELF2B, induces apoptosis in vitro and perturbs early lymphocytic development in vivo. *J. Hematol. Oncol.* **10,** 75
28. Wang, X. M., Yu, D. M. T., McCaughan, G. W., and Gorrell, M. D. (2005) Fibroblast activation protein increases apoptosis, cell adhesion and migration by the LX-2 human stellate cell line. *Hepatology* **42,** 935–945
29. Tholen, S., Biniossek, M. L., Gessler, A. L., Müller, S., Weisser, J., Kizhakkedathu, J. N., Reinheckel, T., and Schilling, O. (2011) Contribution of cathepsin L to secretome composition and cleavage pattern of mouse embryonic fibroblasts. *Biol. Chem.* **392,** 961–971
30. Tholen, S., Biniossek, M. L., Gansz, M., Gomez-Auli, A., Bengsch, F., Noel, A., Kizhakkedathu, J. N., Boerries, M., Busch, H., Reinheckel, T., and Schilling, O. (2013) Deletion of cysteine cathepsins B or L yields differential impacts on murine skin proteome and degradome. *Mol. Cell. Proteomics* **12,** 611–625
31. Knopf, J. D., Tholen, S., Koczorowska, M. M., De Wever, O., Biniossek, M. L., and Schilling, O. (2015) The stromal cell-surface protease fibroblast activation protein-alpha localizes to lipid rafts and is recruited to invadopodia. *Biochim. Biophys. Acta* **1853,** 2515–2525
32. Kleifeld, O., Doucet, A., auf dem Keller, U., Prudova, A., Schilling, O., Kainthan, R. K., Starr, A. E., Foster, L. J., Kizhakkedathu, J. N., and Overall, C. M. (2010) Isotopic labeling of terminal amines in complex samples identifies protein N-termini and protease cleavage products.

Nat. Biotechnol. **28,** 281–288
33. Kern, U., Wischnewski, V., Biniossek, M. L., Schilling, O., and Reinheckel, T. (2015) Lysosomal protein turnover contributes to the acquisition of TGFbeta-1 induced invasive properties of mammary cancer cells. *Mol. Cancer* **14,** 39
34. Rappsilber, J., Ishihama, Y., and Mann, M. (2003) Stop and go extraction tips for matrix-assisted laser desorption/ionization, nanoelectrospray, and LC/MS sample pretreatment in proteomics. *Anal. Chem.* **75,** 663–670
35. Pedrioli, P. G., Eng, J. K., Hubley, R., Vogelzang, M., Deutsch, E. W., Raught, B., Pratt, B., Nilsson, E., Angeletti, R. H., Apweiler, R., Cheung, K., Costello, C. E., Hermjakob, H., Huang, S., Julian, R. K., Kapp, E., McComb, M. E., Oliver, S. G., Omenn, G., Paton, N. W., Simpson, R., Smith, R., Taylor, C. F., Zhu, W., and Aebersold, R. (2004) A common open representation of mass spectrometry data and its application to proteomics research. *Nat. Biotechnol.* **22,** 1459–1466
36. Craig, R., and Beavis, R. C. (2004) TANDEM: matching proteins with tandem mass spectra. *Bioinformatics* **20,** 1466–1467
37. Martens, L., Vandekerckhove, J., and Gevaert, K. (2005) DBToolkit: processing protein databases for peptide-centric proteomics. *Bioinformatics* **21,** 3584–3585
38. Keller, A., Nesvizhskii, A. I., Kolker, E., and Aebersold, R. (2002) Empirical statistical model to estimate the accuracy of peptide identifications made by MS/MS and database search. *Anal. Chem.* **74,** 5383–5392
39. Nesvizhskii, A. I., Keller, A., Kolker, E., and Aebersold, R. (2003) A statistical model for identifying proteins by tandem mass spectrometry. *Anal. Chem.* **75,** 4646–4658
40. Han, D. K., Eng, J., Zhou, H., and Aebersold, R. (2001) Quantitative profiling of differentiation-induced microsomal proteins using isotope-coded affinity tags and mass spectrometry. *Nat. Biotechnol.* **19,** 946–951
41. Kessner, D., Chambers, M., Burke, R., Agus, D., and Mallick, P. (2008) ProteoWizard: open source software for rapid proteomics tools development. *Bioinformatics* **24,** 2534–2536
42. Schilling, O., and Overall, C. M. (2008) Proteome-derived, database-searchable peptide libraries for identifying protease cleavage sites. *Nat. Biotechnol.* **26,** 685–694
43. Schilling, O., auf dem Keller, U., and Overall, C. M. (2011) Factor Xa subsite mapping by proteome-derived peptide libraries improved using WebPICS, a resource for proteomic identification of cleavage sites. *Biol. Chem.* **392,** 1031–1037
44. Zhang, H., Chen, Y., Wadham, C., McCaughan, G. W., Keane, F. M., and Gorrell, M. D. (2015) Dipeptidyl peptidase 9 subcellular localization and a role in cell adhesion involving focal adhesion kinase and paxillin. *BBA Mol. Cell Res.* **1853,** 470–480
45. Yao, T.-W., Kim, W.-S., Yu, D. M., Sharbeen, G., McCaughan, G. W., Choi, K.-Y., Xia, P., and Gorrell, M. D. (2011) A novel role of dipeptidyl peptidase 9 in epidermal growth factor signaling. *Mol. Cancer Res.* **9,** 948–959
46. Osborne, B., Yao, T.-W., Wang, X. M., Chen, Y., Kotan, L. D., Nadvi, N. A., Herdem, M., McCaughan, G. W., Allen, J., Yu, D. M., Topaloglu, A. K., and Gorrell, M. D. (2014) A rare variant in human fibroblast activation protein associated with ER stress, loss of function and loss of cell surface localisation. *Biochim. Biophys. Acta* **1844,** 1248–1259
47. Chowdhury, S., Chen, Y., Yao, T.-W., Ajami, K., Wang, X. M., Popov, Y., Schuppan, D., Bertolino, P., McCaughan, G. W., Yu, D. M., and Gorrell, M. D. (2013) Regulation of dipeptidyl peptidase 8 and 9 expression in activated lymphocytes and injured liver. *World J. Gastroenterol.* **19,** 2883–2893
48. Swamydas, M., Luo, Y., Dorf, M. E., and Lionakis, M. S. (2015) Isolation of mouse neutrophils. *Curr. Protoc. Immunol.* **110**, 3.20.21–23.20.15
49. Scott, C. L., Zheng, F., De Baetselier, P., Martens, L., Saeys, Y., De Prijck, S., Lippens, S., Abels, C., Schoonooghe, S., Raes, G., Devoogdt, N., Lambrecht, B. N., Beschin, A., and Guilliams, M. (2016) Bone marrow-derived monocytes give rise to self-renewing and fully differentiated Kupffer cells. *Nat Commun* **7,** 10321
50. Wuyts, A., D'Haese, A., Cremers, V., Menten, P., Lenaerts, J. P., De Loof, A., Heremans, H., Proost, P., and Van Damme, J. (1999) NH2- and COOH-terminal truncations of murine granulocyte chemotactic protein-2 augment the in vitro and in vivo neutrophil chemotactic potency. *J. Immunol.* **163,** 6155–6163
51. Poplawski, S. E., Lai, J. H., Li, Y., Jin, Z., Liu, Y., Wu, W., Wu, Y., Zhou, Y., Sudmeier, J. L., Sanford, D. G., and Bachovchin, W. W. (2013) Identification of selective and potent inhibitors of fibroblast activation protein and prolyl oligopeptidase. *J. Med. Chem.* **56,** 3467–3477
52. Chowdhury, S., Zhang, H. E., Song, S., Gall, M., Wang, X., Yu, D., Lay, A., Kebebe, M., Lau, B., Evans, K., Liu, Y., Lo, L., Cooney, G., McLennan, S., Turner, N., McCaughan, G., Twigg, S., and Gorrell, M. (2018) Fibroblast activation protein deficiency prevents liver steatosis and insulin resistance and increases fat burning in diet induced obese mice. submitted
53. Vizcaino, J. A., Deutsch, E. W., Wang, R., Csordas, A., Reisinger, F., Rios, D., Dianes, J. A., Sun, Z., Farrah, T., Bandeira, N., Binz, P. A., Xenarios, I., Eisenacher, M., Mayer, G., Gatto, L., Campos, A., Chalkley, R. J., Kraus, H. J., Albar, J. P., Martinez-Bartolome, S., Apweiler, R., Omenn, G. S., Martens, L., Jones, A. R., and Hermjakob, H. (2014) ProteomeXchange provides globally coordinated proteomics data submission and dissemination. *Nat. Biotechnol.* **32,** 223–226
54. Baker, P. R., and Chalkley, R. J. (2014) MS-viewer: a web-based spectral viewer for proteomics results. *Mol. Cell. Proteomics* **13,** 1392–1396
55. Park, J., Knott, H. M., Nadvi, N. A., Collyer, C. A., Wang, X. M., Church, W. B., and Gorrell, M. D. (2008) Reversible inactivation of human dipeptidyl peptidases 8 and 9 by oxidation. *Open Enz. Inhib. J.* **1,** 52–61
56. Zhang, H., Chen, Y., Keane, F. M., and Gorrell, M. D. (2013) Advances in understanding the expression and function of dipeptidyl peptidase 8 and 9. *Mol. Cancer Res.* **11,** 1487–1496
57. Kleifeld, O., Doucet, A., Prudova, A., auf dem Keller, U., Gioia, M., Kizhakkedathu, J. N., and Overall, C. M. (2011) Identifying and quantifying proteolytic events and the natural N terminome by terminal amine isotopic labeling of substrates. *Nat. Protocols* **6,** 1578–1611
58. Shahinian, H., Loessner, D., Biniossek, M. L., Kizhakkedathu, J. N., Clements, J. A., Magdolen, V., and Schilling, O. (2014) Secretome and degradome profiling shows that Kallikrein-related peptidases 4, 5, 6, and 7 induce TGFbeta-1 signaling in ovarian cancer cells. *Mol. Oncol.* **8,** 68–82
59. Smyth, G. K. (2004) Linear models and empirical bayes methods for assessing differential expression in microarray experiments. *Stat. Appl. Genet. Mol. Biol.* **3,** Article 3
60. Schwammle, V., Leon, I. R., and Jensen, O. N. (2013) Assessment and improvement of statistical tools for comparative proteomics analysis of sparse data sets with few experimental replicates. *J. Proteome Res.* **12,** 3874–3883
61. Fortelny, N., Cox, J. H., Kappelhoff, R., Starr, A. E., Lange, P. F., Pavlidis, P., and Overall, C. M. (2014) Network analyses reveal pervasive functional regulation between proteases in the human protease web. *PLos Biol.* **12**, e1001869
62. Shahinian, H., Tholen, S., and Schilling, O. (2013) Proteomic identification of protease cleavage sites: cell-biological and biomedical applications. *Expert Rev. Proteomics* **10,** 421–433
63. Koczorowska, M. M., Tholen, S., Bucher, F., Lutz, L., Kizhakkedathu, J. N., De Wever, O., Wellner, U. F., Biniossek, M. L., Stahl, A., Lassmann, S., and Schilling, O. (2016) Fibroblast activation protein-α, a stromal cell surface protease, shapes key features of cancer associated fibroblasts through proteome and degradome alterations. *Mol. Oncol.* **10,** 40–58
64. Edosada, C. Y., Quan, C., Wiesmann, C., Tran, T., Sutherlin, D., Reynolds, M., Elliott, J. M., Raab, H., Fairbrother, W., and Wolf, B. B. (2006) Selective inhibition of fibroblast activation protein protease based on dipeptide substrate specificity. *J. Biol. Chem.* **281,** 7437–7444
65. Whary, M. T., Baumgarth, N., Fox, J. G., and Barthold, S. W. (2015) Biology and Diseases of Mice. In: Fox, J. G., ed. *Laboratory Animal Medicine*, 3 Ed., pp. 43–149, Academic Press, Boston
66. Barker, H. E., Cox, T. R., and Erler, J. T. (2012) The rationale for targeting the LOX family in cancer. *Nat. Rev. Cancer* **12,** 540–552
67. Ikenaga, N., Peng, Z.-W., Vaid, K. A., Liu, S. B., Yoshida, S., Sverdlov, D. Y., Mikels-Vigdal, A., Smith, V., Schuppan, D., and Popov, Y. V. (2017) Selective targeting of lysyl oxidase-like 2 (LOXL2) suppresses hepatic fibrosis progression and accelerates its reversal. *Gut* **66,** 1697–1708
68. Maruhashi, T., Kii, I., Saito, M., and Kudo, A. (2010) Interaction between Periostin and BMP-1 Promotes Proteolytic Activation of Lysyl Oxidase. *J. Biol. Chem.* **285,** 13294–13303
69. Fan, M.-H., Zhu, Q., Li, H.-H., Ra, H.-J., Majumdar, S., Gulick, D. L., Jerome, J. A., Madsen, D. H., Christofidou-Solomidou, M., Speicher, D. W., Bachovchin, W. W., Feghali-Bostwick, C., and Puré, E. (2016) Fibroblast activation protein (FAP) accelerates collagen degradation and

clearance from lungs in mice. *J. Biol. Chem.* **291,** 8070–8089
70. He, R., Yang, X., Lin y, Shi, Y.-H., Li, B., Liu, W., Yin, W., Dang, Y., Chu, Y., and Fan, J. (2016) FAP promotes immunosuppression by cancer-associated fibroblasts in the tumor microenvironment via STAT3-CCL2 signaling. *Cancer Res.* **76,** 4124–4135
71. Lee, H.-O., Mullins, S., Franco-Barraza, J., Valianou, M., Cukierman, E., and Cheng, J. (2011) FAP-overexpressing fibroblasts produce an extracellular matrix that enhances invasive velocity and directionality of pancreatic cancer cells. *BMC Cancer* **11,** 245
72. Egger, C., Cannet, C., Gérard, C., Suply, T., Ksiazek, I., Jarman, E., and Beckmann, N. (2017) Effects of the fibroblast activation protein inhibitor, PT100, in a murine model of pulmonary fibrosis. *Eur. J. Pharmacol.* **809,** 64–72
73. Jiang, G.-M., Xu, W., Du, J., Zhang, K.-S., Zhang, Q.-G., Wang, X.-W., Liu, Z.-G., Liu, S.-Q., Xie, W.-Y., Liu, H.-F., Liu, J.-S., and Wu, B.-P. (2016) The application of the fibroblast activation protein α-targeted immunotherapy strategy. *Oncotarget* **7,** 33472–33482
74. Lee, T.-H., McKleroy, W., Khalifeh-Soltani, A., Sakuma, S., Lazarev, S., Riento, K., Nishimura, S. L., Nichols, B. J., and Atabai, K. (2014) Functional genomic screen identifies novel mediators of collagen uptake. *Mol. Biol. Cell* **25,** 583–593
75. Surette, A. P., Madureira, P. A., Phipps, K. D., Miller, V. A., Svenningsson, P., and Waisman, D. M. (2011) Regulation of fibrinolysis by S100A10 in vivo. *Blood* **118,** 3172–3181
76. Artym, V. V., Kindzelskii, A. L., Chen, W. T., and Petty, H. R. (2002) Molecular proximity of seprase and the urokinase-type plasminogen activator receptor on malignant melanoma cell membranes: dependence on beta1 integrins and the cytoskeleton. *Carcinogenesis* **23,** 1593–1601
77. Gorrell, M. D. (2005) Dipeptidyl peptidase IV and related enzymes in cell biology and liver disorders. *Clin. Sci.* **108,** 277–292
78. Kim, K.-H., Chen, C.-C., Alpini, G., and Lau, L. F. (2015) CCN1 induces hepatic ductular reaction through integrin $\alpha(v)\beta(5)$–mediated activation of NF-κB. *J. Clin. Invest.* **125,** 1886–1900
79. Chen, C.-C., Kim, K.-H., and Lau, L. F. (2016) The matricellular protein CCN1 suppresses hepatocarcinogenesis by inhibiting compensatory proliferation. *Oncogene* **35,** 1314–1323
80. Devireddy, L. R., Gazin, C., Zhu, X., and Green, M. R. (2005) A cell-surface receptor for lipocalin 24p3 selectively mediates apoptosis and iron uptake. *Cell* **123,** 1293–1305
81. Wuyts, A., Govaerts, C., Struyf, S., Lenaerts, J. P., Put, W., Conings, R., Proost, P., and Van Damme, J. (1999) Isolation of the CXC chemokines ENA-78, GRO alpha and GRO gamma from tumor cells and leukocytes reveals NH2-terminal heterogeneity - Functional comparison of different natural isoforms. *Eur. J. Biochem.* **260,** 421–429
82. Seldin, M. M., Tan, S. Y., and Wong, G. W. (2014) Metabolic function of the CTRP family of hormones. *Rev. Endocr. Metab. Disord.* **15,** 111–123
83. Murayama, M. A., Kakuta, S., Inoue, A., Umeda, N., Yonezawa, T., Maruhashi, T., Tateishi, K., Ishigame, H., Yabe, R., Ikeda, S., Seno, A., Chi, H.-H., Hashiguchi, Y., Kurata, R., Tada, T., Kubo, S., Sato, N., Liu, Y., Hattori, M., Saijo, S., Matsushita, M., Fujita, T., Sumida, T., and Iwakura, Y. (2015) CTRP6 is an endogenous complement regulator that can effectively treat induced arthritis. *Nat. Comm.* **6,** 8483
84. Takeuchi, T., Adachi, Y., and Nagayama, T. (2011) Expression of a secretory protein C1qTNF6, a C1qTNF family member, in hepatocellular carcinoma. *Anal. Cell. Pathol.* **34,** 113–121
85. Wong, G. W., Wang, J., Hug, C., Tsao, T.-S., and Lodish, H. F. (2004) A family of Acrp30/adiponectin structural and functional paralogs. *Proc. Natl. Acad. Sci. U.S.A.* **101,** 10302–10307
86. Kim, M. J., Lee, W., Park, E. J., and Park, S. Y. (2010) C1qTNF-related protein-6 increases the expression of interleukin-10 in macrophages. *Mol. Cells* **30,** 59–64
87. Deshmane, S. L., Kremlev, S., Amini, S., and Sawaya, B. E. (2009) Monocyte Chemoattractant Protein-1 (MCP-1): An Overview. *J. Interferon Cytokine Res.* **29,** 313–326
88. Ehling, J., Bartneck, M., Wei, X., Gremse, F., Fech, V., Möckel, D., Baeck, C., Hittatiya, K., Eulberg, D., Luedde, T., Kiessling, F., Trautwein, C., Lammers, T., and Tacke, F. (2014) CCL2-dependent infiltrating macrophages promote angiogenesis in progressive liver fibrosis. *Gut* **63,** 1960–1971
89. Gong, J.-H., and Clark-Lewis, I. (1995) Antagonists of monocyte chemoattractant protein 1 identified by modification of functionally critical NH2-terminal residues. *J. Exp. Med.* **181,** 631–640
90. Kitamoto, S., and Egashira, K. (2003) Anti-monocyte chemoattractant protein-1 gene therapy for cardiovascular diseases. *Expert Rev. Cardiovasc. Ther.* **1,** 393–400
91. Severin, I. C., Souza, A. L. S., Davis, J. H., Musolino, N., Mack, M., Power, C. A., and Proudfoot, A. E. I. (2012) Properties of 7ND–CCL2 are modulated upon fusion to Fc. *Protein Eng. Des. Sel.* **25,** 213–222
92. Maruyama, S., Nakamura, K., Papanicolaou, K. N., Sano, S., Shimizu, I., Asaumi, Y., van den Hoff, M. J., Ouchi, N., Recchia, F. A., and Walsh, K. (2016) Follistatin-like 1 promotes cardiac fibroblast activation and protects the heart from rupture. *EMBO Mol. Med.* **8,** 949–966
93. Kersey, P. J., Duarte, J., Williams, A., Karavidopoulou, Y., Birney, E., and Apweiler, R. (2004) The International Protein Index: An integrated database for proteomics experiments. *Proteomics* **4,** 1985–1988